AD-A127 030 A MODEL FOR THE SURFACE WIND FIELD IN COMPLEX TERRAIN 1/1
(U) DAYTON UNIV OH RESEARCH INST P A HAINES ET AL.
JAN 83 ERADCOM/ASL-CR-83-0206-1 DAAD07-80-D-0206

UNCLASSIFIED F/G 4/2 NL

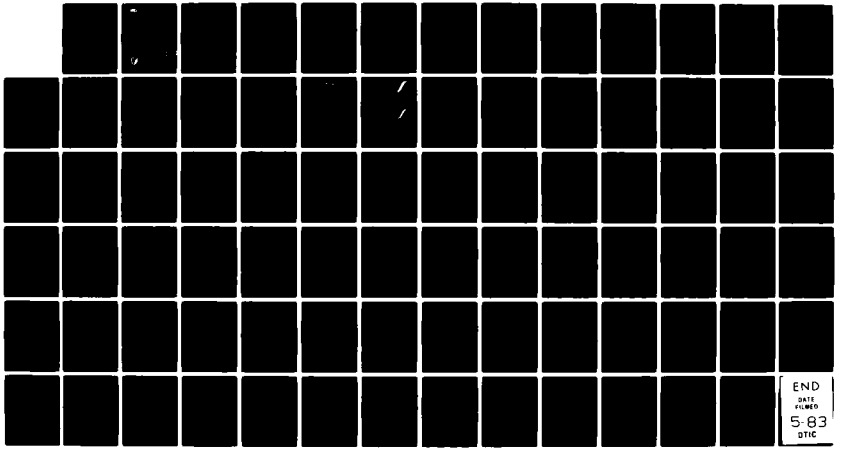

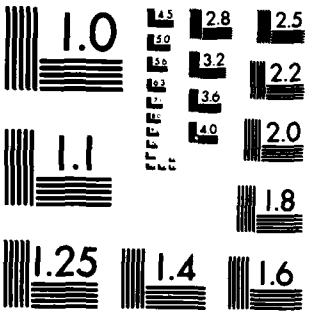

(2)

-CR-83-0206-1

AD
Reports Control Symbol
OSD - 1366

A MODEL FOR THE SURFACE WIND FIELD IN COMPLEX TERRAIN

JANUARY 1983

By

Patrick A. Haines
John L. Keller
Charles D. MacArthur
Jerry G. Jensen

University of Dayton
Research Institute
Dayton, Ohio 45469

Under Contract Number DAAD07-80-D-0206
CONTRACT MONITOR: John T. Marrs

Approved for public release; distribution unlimited.

US Army Electronics Research and Development Command
Atmospheric Sciences Laboratory
White Sands Missile Range, NM 88002

NOTICES

Disclaimers

The findings in this report are not to be construed as an official Department of the Army position, unless so designated by other authorized documents.

The citation of trade names and names of manufacturers in this report is not to be construed as official Government indorsement or approval of commercial products or services referenced herein.

Disposition

Destroy this report when it is no longer needed. Do not return it to the originator.

SECURITY CLASSIFICATION OF THIS PAGE (When Data Entered)

REPORT DOCUMENTATION PAGE		READ INSTRUCTIONS BEFORE COMPLETING FORM
1. REPORT NUMBER ASL-CR-83-0206-1	2. GOVT ACCESSION NO. AD-A127630	3. RECIPIENT'S CATALOG NUMBER
4. TITLE (and Subtitle) A MODEL FOR THE SURFACE WIND FIELD IN COMPLEX TERRAIN		5. TYPE OF REPORT & PERIOD COVERED Final Report 6. PERFORMING ORG. REPORT NUMBER
7. AUTHOR(s) Patrick A. Haines, John L. Keller, Charles D. MacArthur, and Jerry G. Jensen		8. CONTRACT OR GRANT NUMBER(s) DAAD07-80-D-0206
9. PERFORMING ORGANIZATION NAME AND ADDRESS University of Dayton Research Institute Dayton, Ohio 45469		10. PROGRAM ELEMENT, PROJECT, TASK AREA & WORK UNIT NUMBERS
11. CONTROLLING OFFICE NAME AND ADDRESS US Army Electronics Research and Development Command Adelphi, MD 20783		12. REPORT DATE January 1983 13. NUMBER OF PAGES 70
14. MONITORING AGENCY NAME & ADDRESS(if different from Controlling Office) US Army Atmospheric Sciences Laboratory White Sands Missile Range, NM 88002		15. SECURITY CLASS. (of this report) UNCLASSIFIED 15a. DECLASSIFICATION/DOWNGRADING SCHEDULE

16. DISTRIBUTION STATEMENT (of this Report)

Approved for public release; distribution unlimited

17. DISTRIBUTION STATEMENT (of the abstract entered in Block 20, if different from Report)

18. SUPPLEMENTARY NOTES

Contract Monitor: John T. Marrs

19. KEY WORDS (Continue on reverse side if necessary and identify by block number)

Wind flow
Winds in complex terrain
Ryan's model
Terrain analysis for wind flow

20. ABSTRACT (Continue on reverse side if necessary and identify by block number)

A model for calculating terrain-influenced surface (6 meter) wind fields is described. The model determines locally generated slope and valley winds as well as mechanically affected changes in the general wind due to sheltering, diverting, ridge enhancement, and separated flow. A procedure is also given for the generation of an optimal computation grid on which the wind field is computed. Winds calculated on this optimal, and usually

DD FORM 1 JAN 73 1473 EDITION OF 1 NOV 65 IS OBSOLETE

SECURITY CLASSIFICATION OF THIS PAGE (When Data Entered)

20. ABSTRACT (cont)

uneven grid, may then be interpolated by the model to a uniform grid specified by the user. The model is designed to compute wind fields without the need for surface observations. Analysis areas are arbitrary, ranging from as small as 1 km^2 to as large as 50 km^2.

TABLE OF CONTENTS

LIST OF FIGURES

LIST OF FIGURES (continued)

LIST OF TABLES

LIST OF SYMBOLS

N = Number of terrain windows.

l = Window length.

Δl = Window overlap distance.

x = East-West direction.

y = North-South direction.

h = Smoothed height coordinate.

z = Raw height coordinate.

ε = RMS difference between raw and smoothed heights.

σ_z = Standard deviation of raw height field.

f = Efficiency of fit.

S = Local slope.

a = Aspect angle.

y = Slope to horizon.

y_u = Slope to horizon in upwind direction.

y_d = Slope to horizon in downwind direction.

Δh = Difference in terrain height (smoothed).

ΔS = Straight line distance between two points.

h_z = Height of zero curvature point (smoothed).

h_R = Height of ridge point (smoothed).

DH = Elevation distance between smoothed zero curvature point and ridge point.

H_R = Width of ridge.

Ds = Horizontal distance from calculation point to ridge (smoothed).

Y = Valley concavity.

θ = General valley direction.

ε_{max} = nominal maximum value of wind speed difference.

ε_{min} = minimum value of wind speed difference.

N_ε = admissable number of wind speed differences exceeding ε_{max}.

U_g, V_g = East-West and North-South components of geostrophic wind.

U_g^H, V_g^H = Geostrophic wind components at top of transitional layer, H.

H = Height at top of the transitional layer.

Sc = Height at the top of the constant stress layer.

f_o = Coriolis force.

T_c = Temperature at top of constant stress layer, C.

d_b = Distance from grid point to the ocean.

G = Magnitude of geostrophic wind at 50 meters.

b_o = Direction of grid point to ocean.

σ = Stability factor.

R_o = Surface Rossby number.

L = Monin Obuhov stability length.

ψ = Ekman turning of the wind in transitional layer.

u^* = Surface friction velocity.

D_y = Day of the year.

k = Von Karman's constant.

t_d = Time of day.

z_o = Surface roughness height.

ϕ_r = Latitude.

Z_r = Reference height (50 meters).

F_u = Sheltering factor.

W_{sd} = Surface wind speed after correction for sheltering.

U_{sd}, V_{sd} = Component of surface wind with sheltering and diverting correction only.

W_b = Magnitude of general surface wind without terrain corrections.

U_b, V_b = Components of general surface wind without terrain corrections.

F_D = Angular correction of surface wind for diverting.

θ_b = Direction of general surface wind without terrain corrections.

F = Surface friction coefficient.

θ_{sd} = Direction of general surface wind with diverting corrections only.

$W_{\rho s}$ = Magnitude of slope wind parallel to slope.

W_s = Magnitude of slope wind in horizontal plane.

I = Solar insolation.

P_B = Atmospheric transmissivity.

U_s, V_s = Components of slope wind.

h_s = Characteristic ridge or hill height.

l_s = Characteristic ridge or hill length.

$\Delta\Sigma$ = Speed up factor for ridge enhancement.

N_B = Brunt Vaisalla frequency.

F_h = Hill Froude number.

SD = Separation distance for Hill.

CF = Confidence factor for wind corrections.

P_B = Atmospheric transmissivity.

W_v = Magnitude of valley wind.

U_v, V_v = Components of valley wind.

U, V = Components of surface wind after terrain corrections.

W, ϕ = Magnitude and direction of surface wind after terrain corrections.

U_o, V_o, CF_o = First guess mean wind fields for interpolator.

R_f = Radius of influence.

J = Number of non-uniform grid points within radius of influence about a uniform grid point.

d = Distance from uniform to non-uniform grid point.

U', V', CF' = Interpolated value of parameters.

INTRODUCTION

A fundamental requirement for the calculation of transport and diffusion of smoke and contaminants in the lower atmosphere is the specification of the wind field. The direct approach to computing the surface winds by numerically solving the equations of motion of the lower atmosphere is impractical due to both computational restrictions and lack of knowledge of many of the basic processes involved. Most currently used methods for computing the surface wind field rely upon observations; the results produced by interpolating between observed points. The horizontal resolution of these fields is limited by the density of observations.

For tactical field operations there is a need for a model which is able to calculate high resolution surface wind fields over arbitrary terrain without the need for observations. The model should account for the specific influences of day of the year, time of day, atmospheric transmissivity, surface temperature, cloud cover, atmospheric flow and surface roughness. As well, it should be computationally efficient so that it can be used in near real time.

This report describes the development of a surface wind model and associated terrain processing methods designed to meet the above criteria. The method is an extension and improvement of a method originated by Ryan (1974). The basic principle of Ryan's work is to empirically incorporate the commonly observed influences that terrain has on surface winds. Second order interaction between the influences is ignored. This empirical approach while greatly facilitating the computational problem offers realistic winds for transport and diffusion models. In several case studies, the method successfully calculated the time and space variations of winds in complex terrain.

The work proceeded in two primary tasks. Ryan had relied on personal measurement of terrain for use in his method. The

first task supplanted this approach and involved developing the methodology necessary to produce an optimized computation grid from high resolution uniformly gridded terrain height data. The development of the computation grid takes into account the terrain influences on the wind field so that a wind field of any desired resolution can be obtained for all terrain types.

The second task involved the development of the surface wind model which incorporates as many as possible of influences terrain has on the local wind. The model calculates wind vectors on the optimized (and, normally, nonuniform) computation grid produced by the methodology of the first task. The resulting wind field can then be interpolated to a uniform grid of arbitrary resolution as specified by the user.

The details of the algorithms and computer programs formulated for the development of these programs is discussed in the following sections.

SECTION 1
TERRAIN ANALYSIS AND GRID GENERATION (TAGG)

The objective of the terrain analysis and grid generation computer programs is to provide an optimum grid and associated data for the computation of surface wind fields for a given geographic region. The system analyzes terrain height data to select appropriate grid points and then computes the values of the terrain wind parameters (TWPs) for these points. The TWPs are certain data items - slope, aspect, valley direction, etc. -required for calculating local influences on the surface wind. The output of this system, the optimum (and, most likely, nonuniform) grid and associated TWPs, forms a data base for all surface wind computations for the region under consideration.

1.1 GENERAL STRUCTURE

The modular design of the TAGG system is shown in Figure 1. The components are: (1) selection of the analysis region, (2) Tchebyshev polynomial smoothing of the terrain height field, (3) calculation of the terrain wind parameters and (4) determination of the optimum computation grid.

1.2 SELECTION OF THE ANALYSIS REGION

This initial part of the procedure requires user decision-making. The user divides the large-scale map area into overlapping square subregions or "terrain windows." Each subregion, 'n,' will be specified by a length, l. An overlap between adjacent windows will be specified by the parameter Δl. The overlap is required for consistency in the smoothing process which follows. These parameters are constant for all n=N terrain windows. The UTM coordinates for the corners of the large-scale map will also be given by the user.

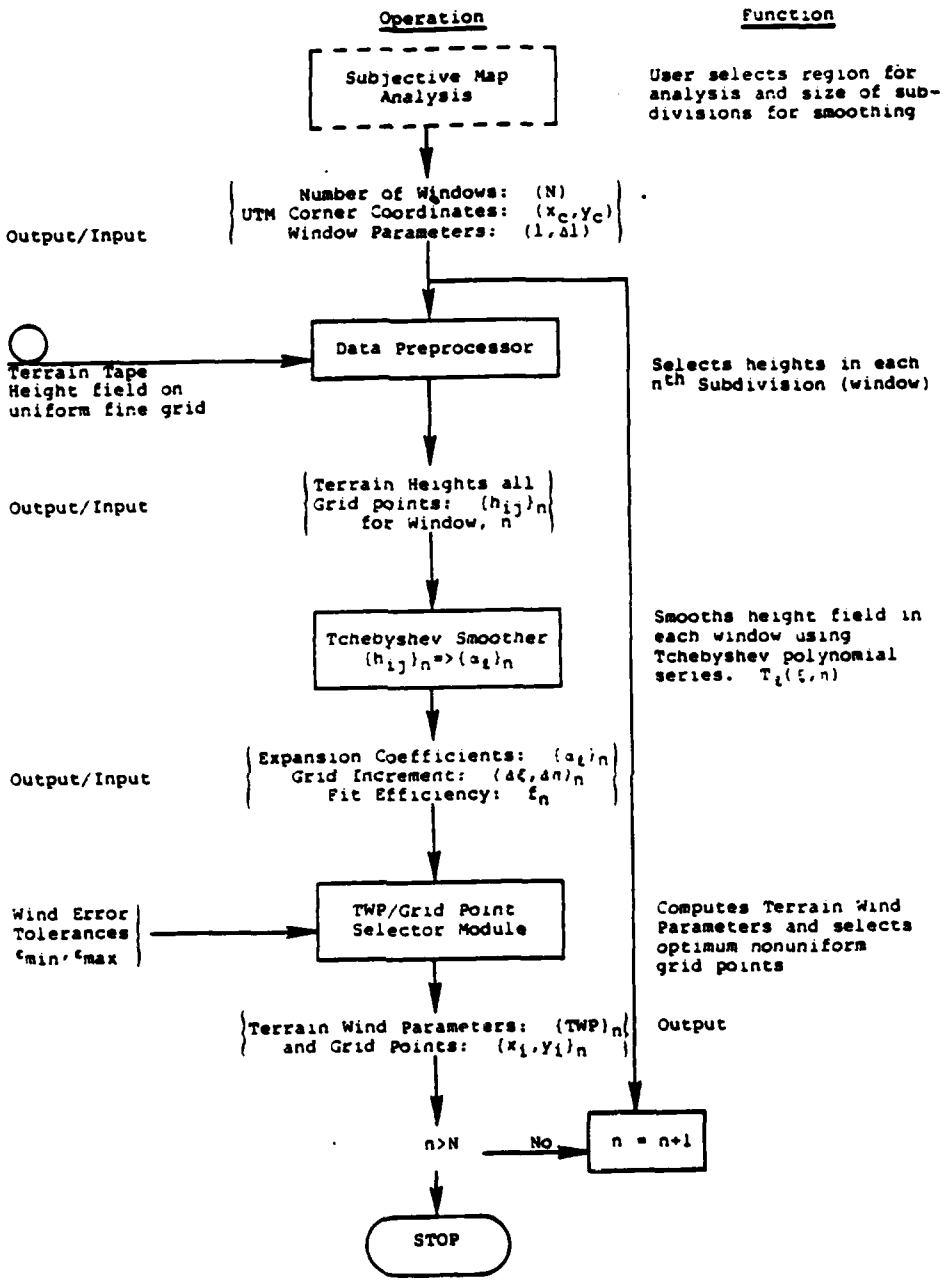

Figure 1. General Software Structure of the Terrain Gridding System.

1.3 TCHEBYSHEV POLYNOMIAL SMOOTHING OF THE TERRAIN

The fourth-order two-dimensional Tchebyshev polynomial was selected to fit a gridded field of terrain heights. A fourth order polynomial in two dimensions may have up to three critical values (slope = 0) along any line of sight through the represented region. Thus the degrees of freedom of the polynomial allows for two peaks and a valley or two valleys and a peak to occur in the smoothed data in any direction. The subjective choice of window size should be based on the horizontal dimensions of important terrain features. No more than two meteorologically significant hills or valleys should be included within the dimension of a single window. This selection enables a large number of terrain heights to be represented by a single polynomial fit. In addition, the fitting removes the small scale terrain "bumps" which are too small to significantly affect the local wind.

Tchebyshev polynomials are advantageous for at least two reasons. First, they are orthonormal, thus their coefficients are readily obtained. Secondly, they are efficient in representing complex terrain because they have infinite order convergence for non-periodic data fields (Boyd, 1978). The latter property is the chief advantage Tchebyshev polynomials have over Fourier series.

The smoothed height field derived by fitting fourth order two-dimensional Tchebyshev polynomials to raw terrain height data is

$$h(x,y) = \sum_{m} \sum_{n} \alpha_{m,n} T_{m,n} \qquad (1)$$

where the Tchebyshev polynomials

$$T_{m,n} = T_m(x)\ T_n(y) \qquad (2)$$

are

$$T_{0,0} = 1$$
$$T_{1,0} = x$$
$$T_{2,0} = 2x^2-1$$
$$T_{3,0} = 4x^3-3x$$
$$T_{4,0} = 8x^{4-8}x^2+1$$
$$T_{0,1} = y$$
$$T_{1,1} = xy$$
$$T_{2,1} = (2x^2-1)y$$
$$T_{3,1} = (4x^3-3x)y$$
$$T_{0,2} = 2y^2-1$$
$$T_{1,2} = x(2y^2-1)$$
$$T_{2,2} = (2x^2-1)(2y^2-1)$$
$$T_{0,3} = (4y^3-3y)$$
$$T_{1,3} = x(4y^3-3y)$$
$$T_{0,4} = 8y^4-8y^2+1$$

and the polynomial coefficients are derived from

$$\alpha_{m,n} = \frac{\sum_{i=0}^{I-1}\sum_{j=0}^{J-1} Z(x,y)\, T_{m,n}(x_i,y_j)}{\sum_{i=0}^{I-1}\sum_{j=0}^{J-1} T_{m,n}^{2}(x_i,y_j)} \qquad (3)$$

where
- Z(x,y): raw terrain height
- i: index in x direction
- j: index in y direction
- I,J: total number of data points in x and y directions respectively.

After the smoothing is performed, the residual or root mean square height differences, ε, between the raw and smoothed height field is calculated. The residual is a measure of the fidelity with which the polynomial series represents the original height field. An efficiency of fit for each window is obtained from the root mean square, ε, and the standard deviation of the raw height

field, σ_z, as

$$f = \frac{\sigma_z^2 - \epsilon^2}{\sigma_z^2} \qquad (4)$$

Qualitatively, a fit efficiency of 0.60 and above represents an adequate fit while an efficiency of 0.85 and above means an excellent fit.

Subjective map analysis is recommended so that the window size is chosen to best characterize the terrain features. The smoothing which occurs as a consequence of the fit can then work to the user's advantage for filtering out irrelevent details in the terrain.

Figures 2 and 3 compare actual and fitted height fields for two idealized terrain surfaces. Respectively, they are a cosine shaped knoll and a cosine shaped valley. The general characteristics of each surface is reasonably conserved. Note that in the cosine knoll case, which is surrounded by a flat region, an upward sloping region occurs near the corners. Figures 4 and 5 compare an actual terrain height field (shown as the deviation from the mean elevation) with its Tchebyshev polynomial representation. While smoothing is evident, the general complexity of the original terrain is preserved by the fitting. The efficiency of fit, f_n, for this case is 0.822.

In practice a sizeable number of individual terrain fits may be required to represent an area of interest. A mosaic of overlapping fit windows is used to produce a relatively continuous, smoothed terrain surface. Centered within each window is a region of computational validity where the wind vectors are calculated called a cell (see figure below). The window overlapping prevents sharp discontinuities that might otherwise occur at the boundaries between adjacent windows. In the cosine knoll case for example, the upward sloping regions near the

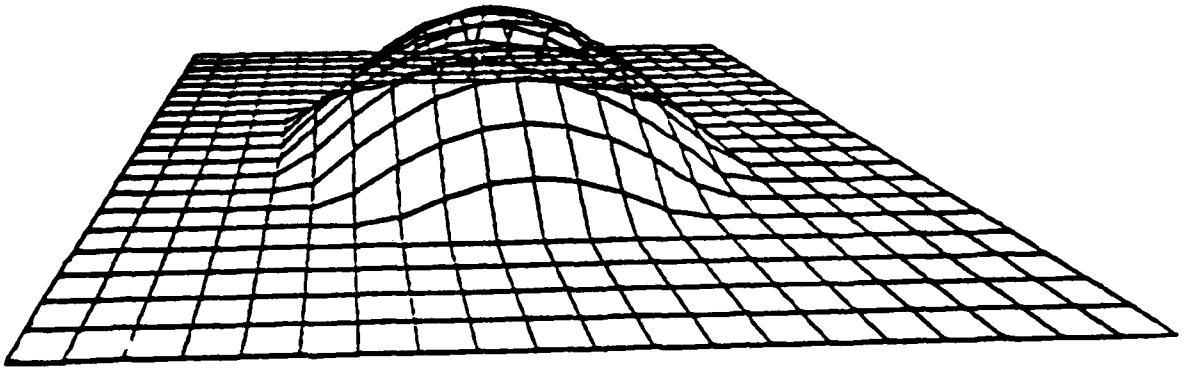

COSINE KNOLL: "RAW" HEIGHT FIELD

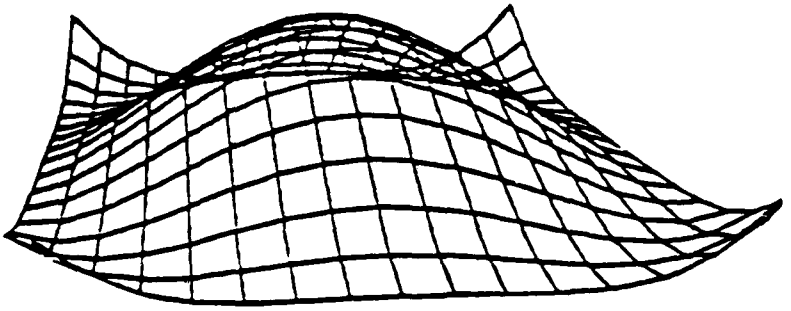

COSINE KNOLL: TCHEBYSHEV FIT WITH 1.6 km WINDOW

Figure 2. Idealized Raw and Smoothed Cosine Height Field.

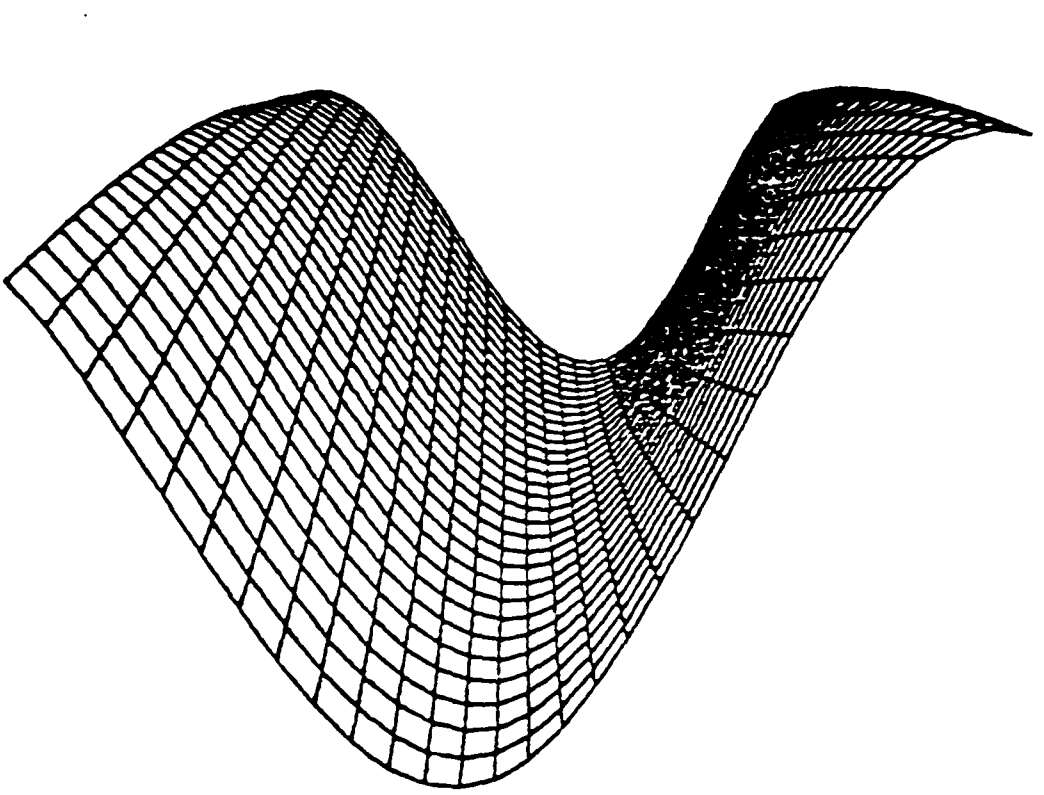

COSINE SHAPED VALLEY: "RAW" HEIGHT FIELD

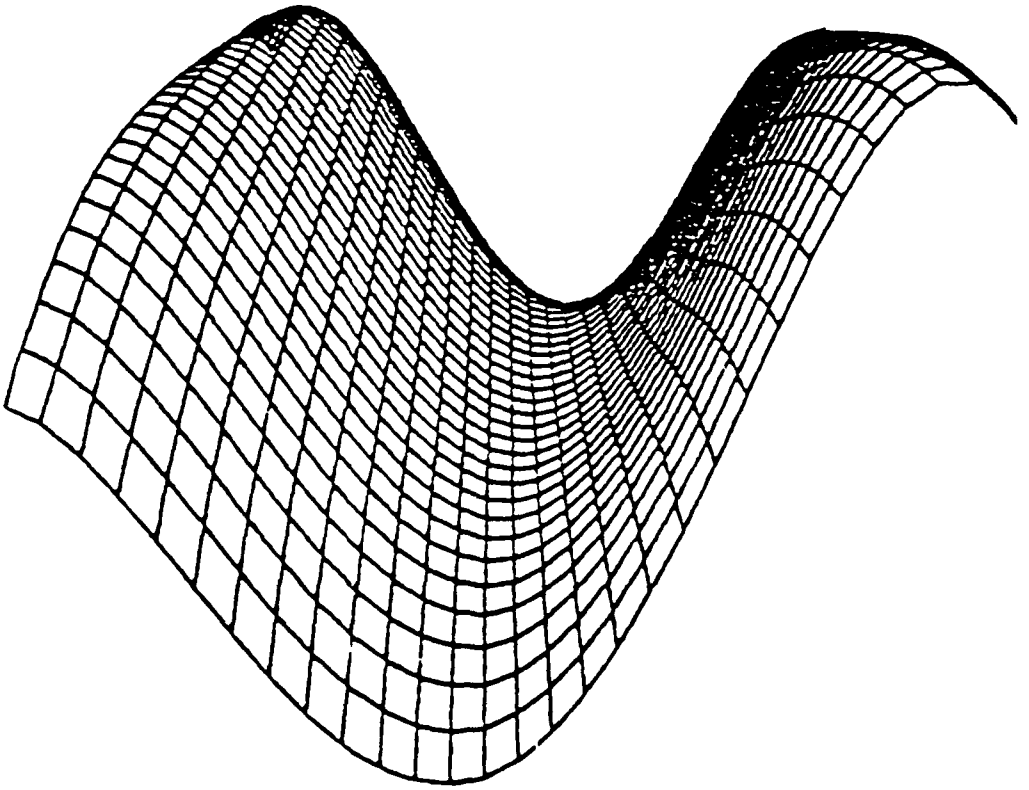

COSINE SHAPED VALLEY: FITTED FIELD WITH 2km WINDOW

Figure 3. Raw and Smoothed Cosine Shaped Valley.

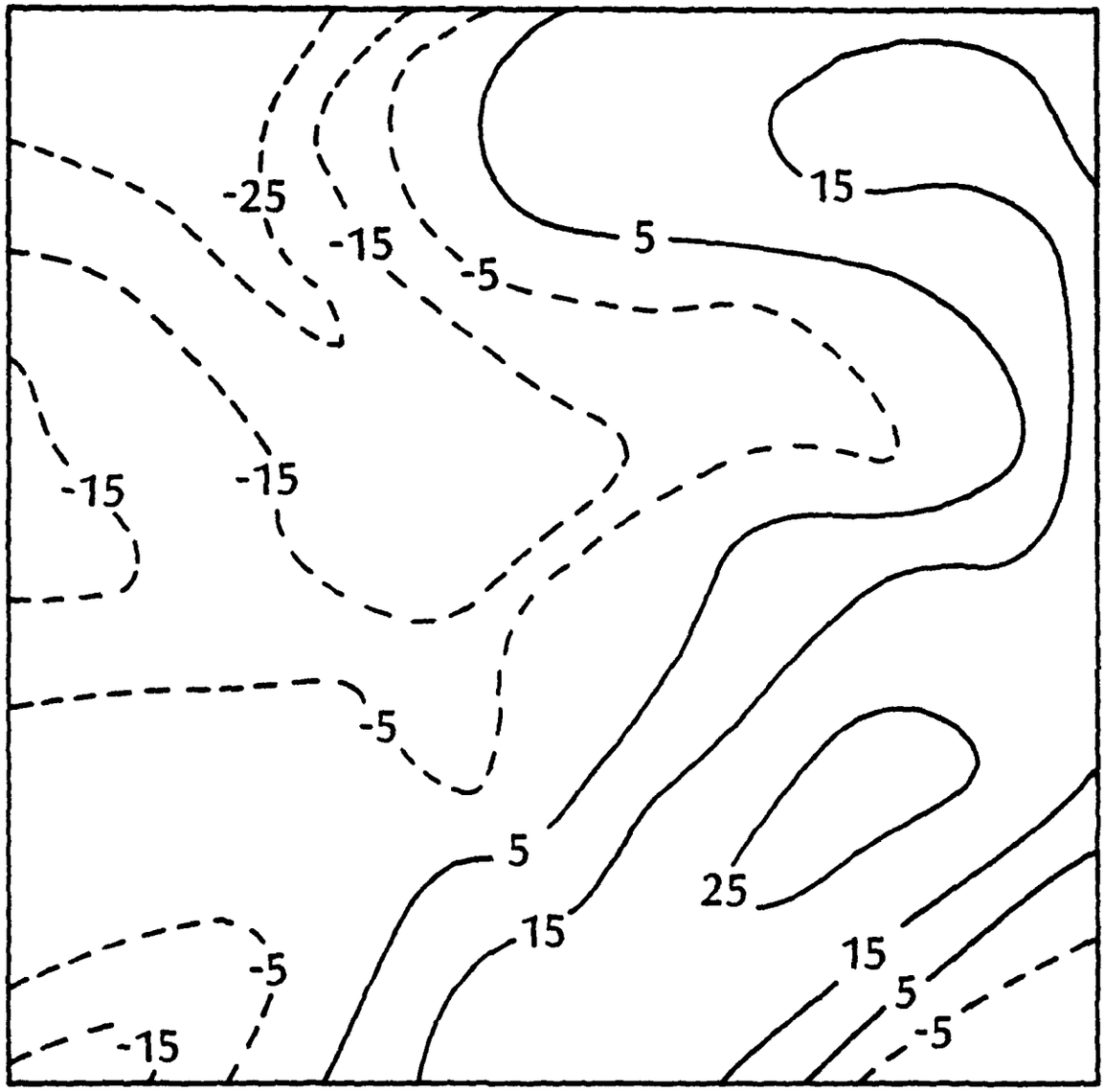

Figure 4. Sample of Actual Terrain Surface.

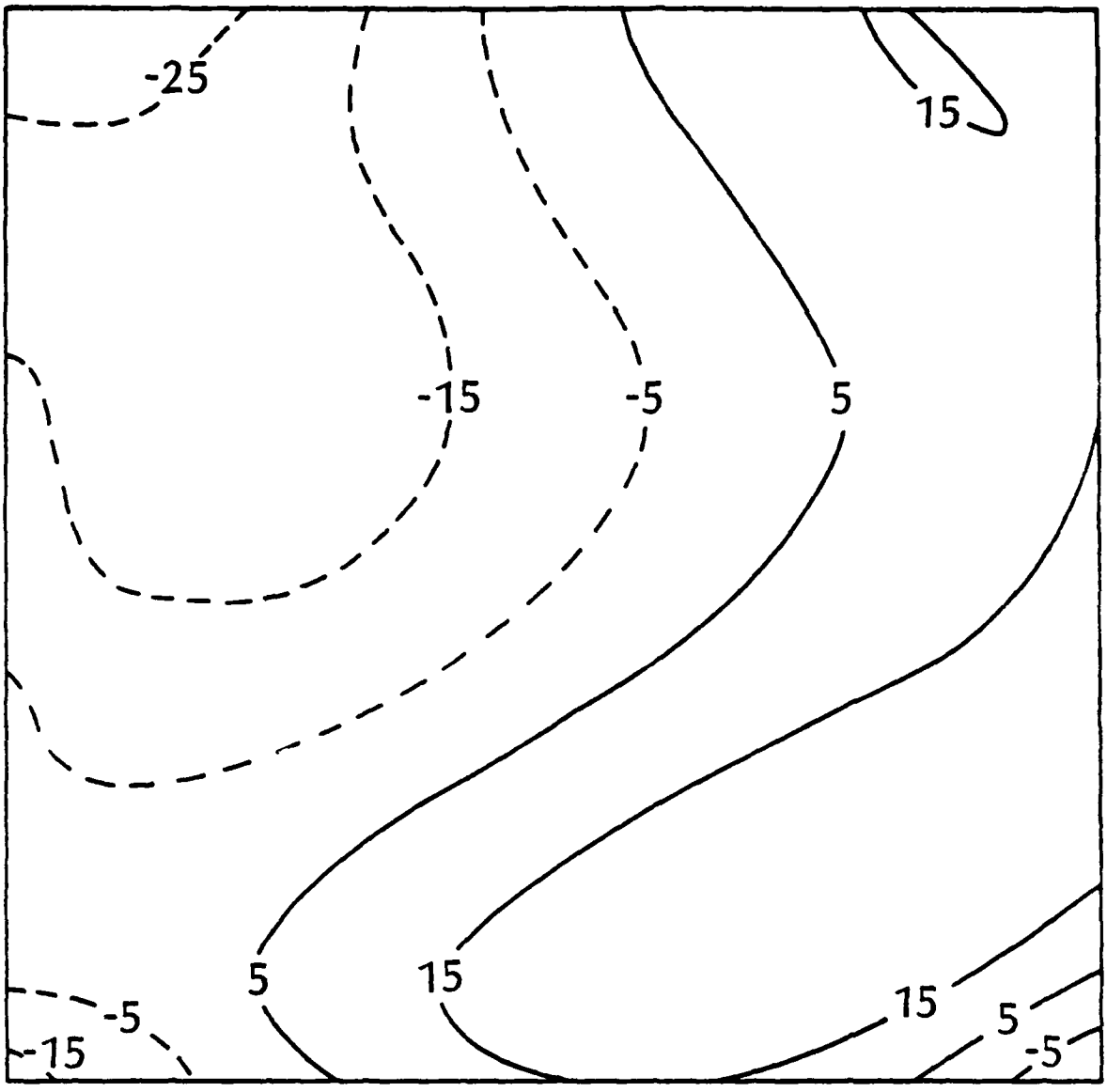

Figure 5. Smoothed Terrain Surface, f = 0.822.

corners would not be used in wind computations since they would not be within the cell.

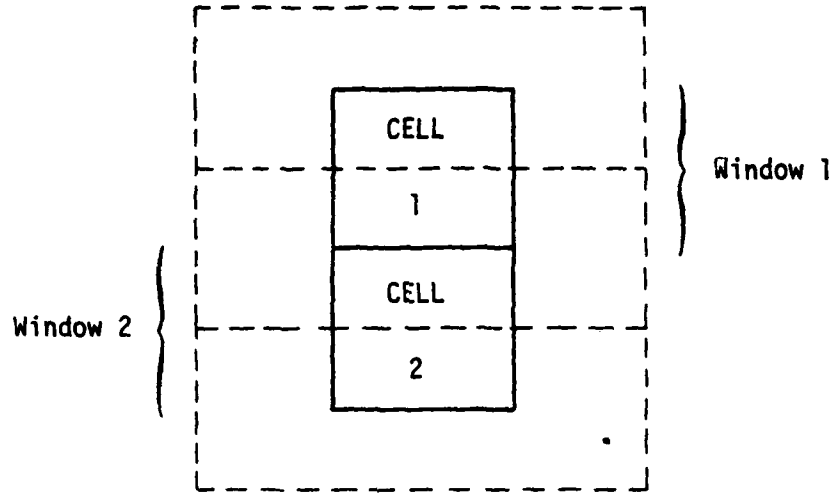

1.4 TERRAIN WIND PARAMETER (TWP) GENERATION

The wind field at each grid point is influenced by certain terrain parameters of its surroundings. These Terrain Wind Parameters (TWPs) are derived from the Tchebyshev polynomial representation of the terrain surface. For the polynomial representation of a window, TWPs are calculated only at grid points within the cell boundaries as discussed in the previous section. The TWPs, since they describe terrain features, need to be calculated only once for any given cell. The ability to calculate many wind fields without the need to handle the basic terrain height data each time greatly reduces computer costs. As well, the analytical representation of the terrain surface allows for a more straightforward determination of the TWPs. The following paragraphs discuss the definition and calculation of each TWP.

Local Slope, S.

The local slope S at a grid point is the modulus of the local terrain gradient, i.e.,

$$S = |\nabla h| = \{ \left(\frac{\partial h}{\partial x} \right)^2 + \left(\frac{\partial h}{\partial y} \right)^2 \}^{1/2} \qquad (5)$$

It is calculated directly from the polynomial expression for the terrain height surface.

Aspect Angle, a.

The aspect angle at a point is the direction towards which the tangent plane is facing. It is defined such that a slope (Plane) facing southward has an aspect angle of 180°. A slope facing northward: 0°. The aspect angle can be seen to be equivalent to the compass direction opposite to the direction of the terrain gradient vector, ∇h. Hence

$$a = \pi/2 - \tan^{-1} \left(\frac{\partial h/\partial y}{\partial h/\partial x} \right), \qquad (6)$$

$$\text{if } a < 0 \quad a = a + 2\pi$$

Upwind and Downwind Slope to Horizon, Y.

At each grid point (x,y) with smoothed height coordinate, h, the slope to horizon, Y, is calculated in the eight primary compass directions. We use

$$Y = (\Delta h/\Delta s)_{max} \qquad (7)$$

where $\Delta h = h_p - h$ (8)

and $\Delta s = [(x_p - x)^2 + (y_p - y)^2]^{1/2}$ (9)

The slope is calculated between the point (x,y) and every other grid point (x_p, y_p) in the specified direction, the maximum value of $\Delta h/\Delta s$ along a specified compass direction defines the horizon. The eight compass directions are defined to be along lines of constant x, constant y, and $x=\pm y$. The coordinate system is defined such that increasing x is eastward and increasing y is northward. Depending on the direction of the general wind, the

appropriate upwind and downwind values, Y_u and Y_d, are selected from the eight values in the set {Y}.

Ridge Parameters, Dh, Ds, H_R.

Ridge parameters are calculated for those points that lie in the vicinity of a ridge. More explicitly, the parameters Dh, Ds, and H_R are calculated for those points that lie between the zero curvature point (concavity change from valley to ridge) and the ridge line point. The ridge line point in a specified direction is derived from the gradient of the smoothed terrain elevation in that direction. The gradient is a cubic polynomial in x,y coordinates and is then transformed into polar r, ϕ, coordinates with origin at the grid point of calculation. Thus

$$r \cdot \nabla h = \cos \phi \frac{\partial h}{\partial x} + \sin \phi \frac{\partial h}{\partial y} = A_o + A_1 r + A_2 r^2 + A_3 r^3 \qquad (10)$$

where $r = i \cos \phi + j \sin \phi$: unit radial vector

ϕ : clockwise angle from North

r : radial coordinate

The real roots of the above expression are evaluated for each of eight compass directions.

The parameter Dh is the elevation difference between the zero curvature point, h_z, and the ridge line in a specified direction, that is:

$$Dh = | h_R - h_z | \qquad (11)$$

where H_R : smoothed value of elevation at the ridge line,

The parameter Ds is the straight line horizontal distance from the calculation point to the ridge line in a specified direction, i.e.

$$s = [(x - x_R)^2 + (y - y_R)^2]^{1/2} \qquad (12)$$

where x_R, y_R : coordinates of the point on ridge line in the specified direction.

The roots $\{r_o\}$ of the cubic correspond to either a point on the valley line or ridge line in the direction ϕ from the grid point of calculation. A valley line point is discriminated from a ridge line point by the sign of the partial derivative of the gradient.

$$\frac{\partial}{\partial r}(r \cdot \nabla h) = (A_1 + 2A_2 r + 3A_3 r^2)\Big|_{r=r_o} \quad \begin{matrix} < 0, \text{ Ridge} \\ > 0, \text{ Valley} \end{matrix} \qquad (13)$$

The parameter H_R is a measure of the ridge width in a specified direction. The ridge width is the distance in the horizontal plane between the ridge line point and the zero curvature point (x_z, y_z). The zero curvature point is the real root of the equation,

$$A_1 + 2A_2 r + 3A_3 r^2 = 0 \qquad (14)$$

that lies between the calculation point and the valley line point. The ridge width is calculated in each of up to eight directions as:

$$H_R = [(x_R - x_z)^2 + (y_R - y_z)^2]^{1/2} \qquad (15)$$

The ridge parameters are used to calculate enhanced wind speed for grid points lying on the upper half of a hill. No ridge parameter are calculated for points on the lower half (i.e., below the zero curvature point in a valley). Ridge points are calculated in each of eight compass directions when possible. In many cases a ridge point will not be found in certain directions in which case no parameters are calculated.

General Valley Direction, θ.

The general valley direction θ, is the upvalley direction of the "dominant" valley within the cell (non-overlapping part)

of a window. The choice of resolution or window size used in fitting the Tchebyshev polynomials to the original grid of terrain heights should be such that the cell size is on the order of the dimensions of a valley. At each grid point within the cell the average valley direction of the entire cell is assigned. The average direction is the vector mean of the individual valley directions at each grid point. The calculation of an individual valley direction at a point begins by looking in the four directions (N,E,S,W) for the closest valley point. The valley points are determined from the roots of the polynomial in a similar fashion to finding a ridge point. At the closest valley point a search is made in 10° increments for the direction of greatest elevation decrease. The individual valley direction at the grid point is then defined to be 180° from the direction of greatest elevation decrease.

Valley Concavity, $\bar{Y}$.

The valley concavity, $\bar{Y}$ is a measure of the "valleyness" of the valley at an arbitrary grid point. The equation for valley concavity is

$$\bar{Y} = (Y_l + Y_r)/2$$

where Y_l and Y_r are the slopes to the horizon to the left and right of the general valley direction. The slopes to the horizon are derived the same way as the general slope to the horizon (Equation 7).

1.5 DETERMINATION OF THE OPTIMUM WIND COMPUTATION GRID

The construction of an optimum computation grid is a two step process. The first step is the construction of a uniform grid of sufficient resolution. The second step is to remove all unnecessary grid points from the uniform grid. The resulting grid is nonuniform, due to the removal of some of the uniform grid points, and optimal since no more points can be removed. The overall process is driven by three user specified input values--ε_{max}, ε_{min}, and N_ε.

In the first step of constructing a uniform grid of sufficiently fine resolution, the two values ϵ_{max} and N_ϵ are used. ϵ_{max} is the nominal maximum permissible value of wind speed difference, ΔV, between any two adjacent grid points. However, this restriction is relaxed to the extent that up to N_ϵ values of ΔV may exceed ϵ_{max}.

The uniform grid is constructed in the following manner. The program begins by constructing a four by four grid of test points to represent a terrain cell (a cell is the nonoverlapping portion of the Tchebyshev window). The program then computes the terrain wind parameters at each of the sixteen grid points. For each grid point the program then computes the value of ΔV (see Section 2) between it and its right and top neighbor (except for the right column and top row of points). If a value of ΔV exceeds ϵ_{max} a counter is incremented and a check is made to see if the counter values exceeds N_ϵ. If this happens, then the program "knows" the grid resolution is not fine enough (i.e., the number of ΔV, exceeding ϵ_{max} $> N_\epsilon$). In such a case the program doubles the grid resolution (four by four becomes an eight by eight) and starts the process again.

If after computing ΔVs for all the grid points, the number of "too big" ΔVs does not exceed N_ϵ then the program accepts the current grid resolution as being sufficiently fine. It should be noted that the program will continue doubling the grid resolution, if necessary, up to a maximum of 64 by 64 grid points. If such a resolution is still not fine enough, the program will print an error message proclaiming this condition and continue on with the grid optimization procedure. The program will utilize the 64 by 64 grid even though this grid does not satisfy the ϵ_{max} and N_ϵ criteria.

Once a fine enough uniform grid has been constructed, the program proceeds to remove all unnecessary grid points. This process is controlled by the user input value ϵ_{min}. A grid point

is deleted from the grid if the values of ΔV between the point and its upper, right, lower, and left neighbors are less than ϵ_{min}. Each point in the grid is tested for this condition and deleted if possible. After the first deletion pass through the grid, some of the remaining grid points have new neighbors due to the deletion of their original neighbors. A second deletion pass is made through the now sparser grid to delete any of the remaining grid points that also satisfy the deletion criteria with their new neighbors. Deletion passes through the grid are repeated until a deletion pass is made in which no grid points are deleted. This means that no grid points get new neighbors, thus no new ΔVs will be computed which could be less than ϵ_{min} and the deletion process is completed. The grid points that remain comprise the optimal nonuniform grid.

It should be noted that the deletion process can be "turned off" by the user by entering an input value of 0 for ϵ_{min}. Since ΔV is always greater than or equal to 0, no points will be deleted. Likewise the user can "force" the program to accept a four by four grid every time by entering a value N_ϵ greater than 32. Since the program only checks the values of ΔV to the top and right neighbors of a grid point, a maximum of 32 "too big" ΔVs can occur.

To test and evaluate the grid optimization procedure, a synthetic terrain data base was generated that represents a three dimensional cosine curve. To test the optimization procedure the wind difference criteria, ΔV, was replaced by the easily calculable height difference between the points. Because this was a test of the optimization process and not of the grid construction process, a grid of 130 by 130 points was constructed, which correspond to an ϵ_{max} of .2 altitude units. In this test case, the program increased the grid resolution by ten times at each step rather than doubling the resolution. Figures 6, 7, and 8 show this grid after optimization corresponding to ϵ_{min} values of .05, .1, and .2 respectively. It can be observed from these

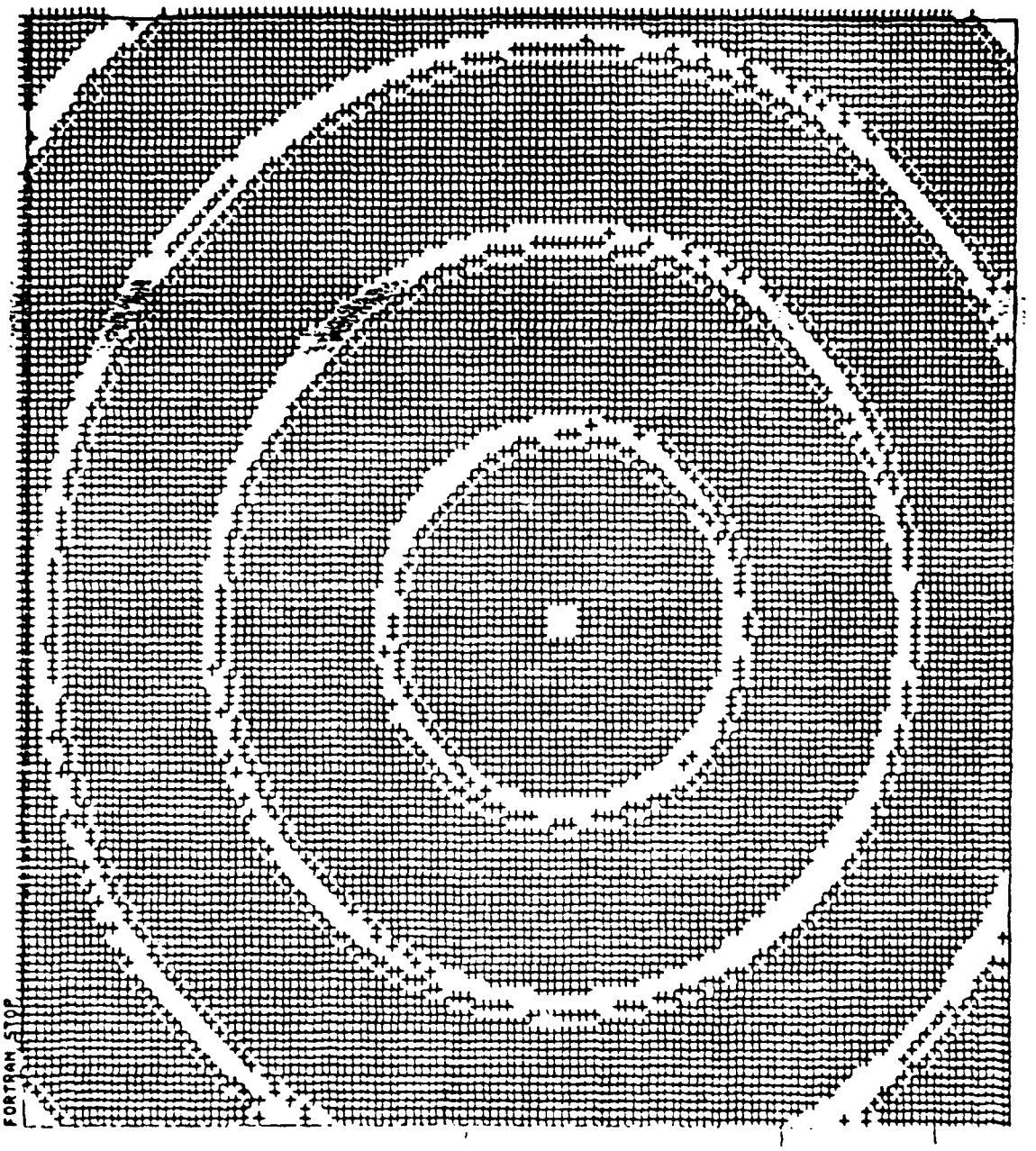

Figure 6. Sample of Grid Optimization Output for Cosine Shaped Terrain. $\Sigma_{max} = .2$, $\Sigma_{min} = .05$.

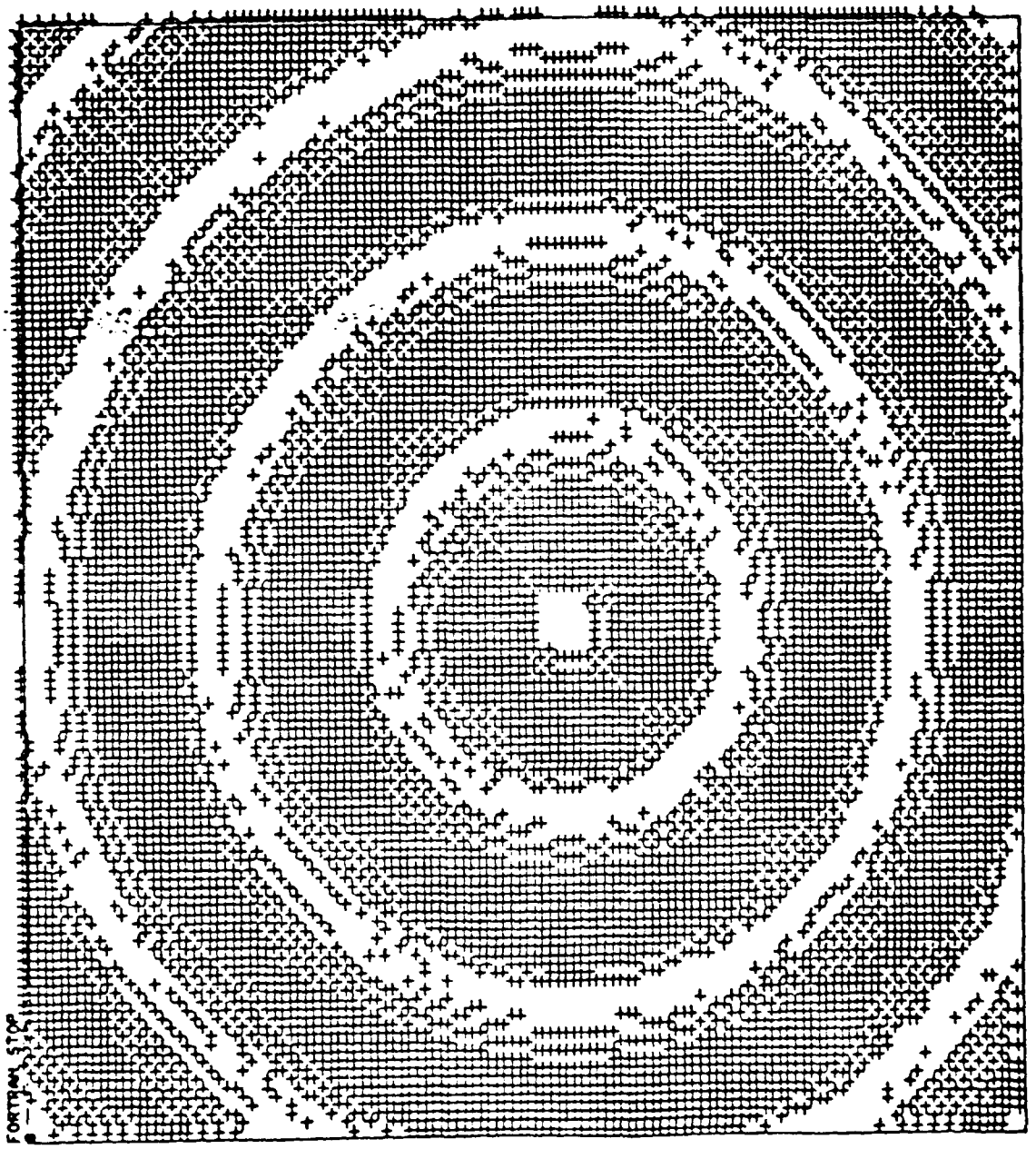

Figure 7. Sample of Grid Optimization Output for Cosine Shaped Terrain. $\Sigma_{max} = .2$, $\Sigma_{min} = .1$.

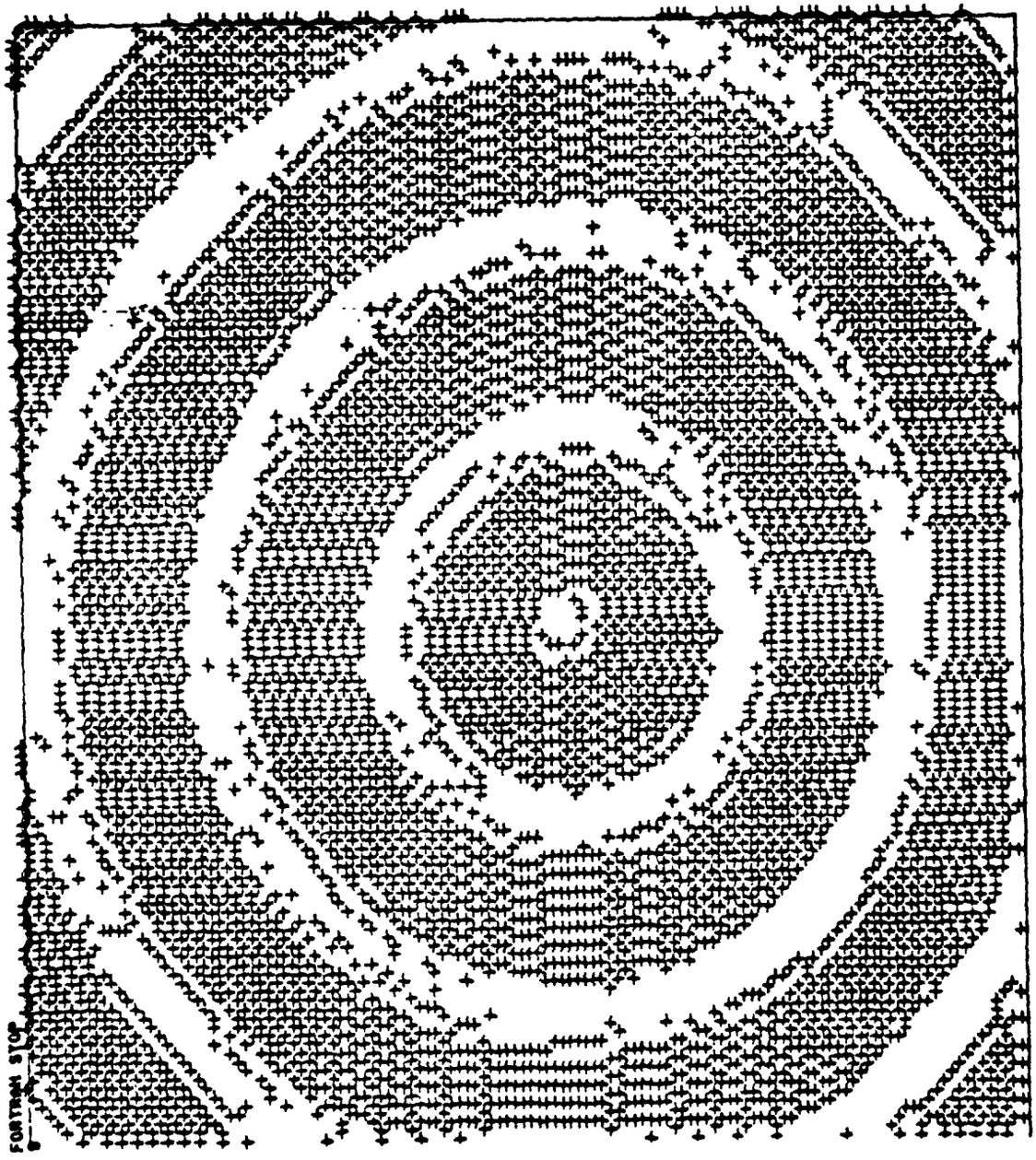

Figure 8. Sample of Grid Optimization Output for Cosine Shaped Terrain. $\Sigma_{max} = .2$, $\Sigma_{min} = .2$.

figures that an increasing value of ε_{min} will cause the resultant optimal grid to thin out. Note that the areas with no points correspond to the peaks and troughs of the cosine curve where the altitude difference between points is small.

SECTION 2
THE SURFACE WIND MODEL

The Surface Wind Model (SWM) calculates the surface winds over a specified region on the optimal computation grid. In order to make wind calculations at each grid point it is necessary to know the terrain wind parameters (TWPs) and surface roughness at each grid point, the latitude, longitude, cloud cover and transmissivity for the specified region, and the time and date. The procedure for using these parameters to derive surface winds is described below. The resulting wind field on the nonuniform grid is interpolated to a uniform grid for final presentation.

The SWM consists of three main components (Figure 9). The first component involves the calculation of the atmospheric stability and general surface wind from the free atmospheric wind (at about the 1500 m or the 850 mb level). The general surface wind is obtained for each square kilometer of the analysis region. The resulting wind vectors are passed to component 2 which calculates the six terrain perturbations to the general surface wind. The perturbations are calculated at each grid point using the TWPs associated with that point. The six perturbations are vectorially added to the general surface wind for the appropriate square kilometer to give a resultant local surface wind at each grid point. The third component of the surface wind model, the interpolator converts the wind field from a nonuniform grid to a use specified uniform grid for output and display purposes.

2.1 INPUT

Input to the surface wind model, as shown in Table 1, comes from three sources: the terrain and TWP output from the terrain grid analysis, aerodynamic surface roughness values for each square Kilometer region, and input describing the meteorological condition for the time of wind calculations. The optimum non-

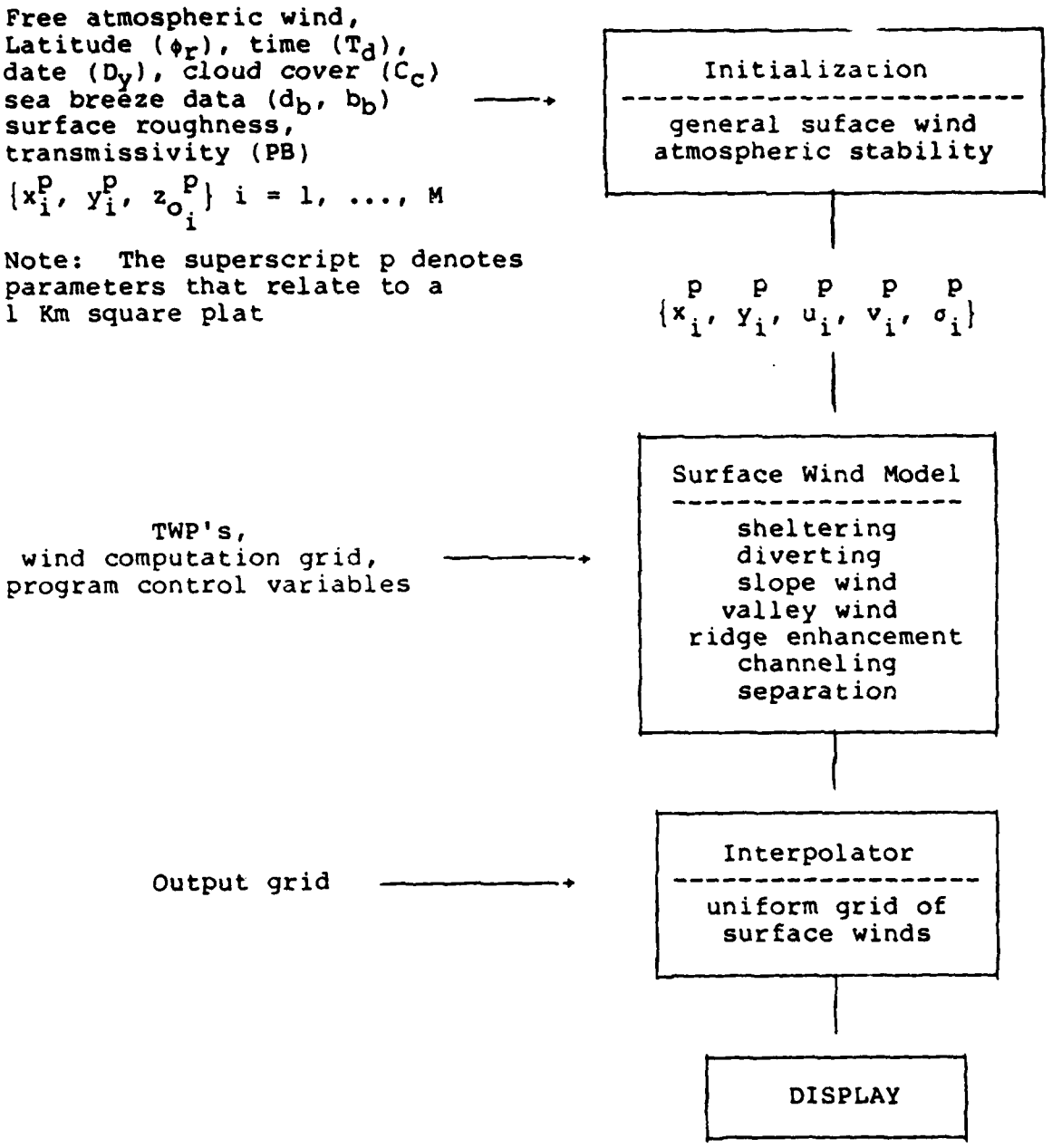

Figure 9. Surface Wind Model.

uniform grid, the raw terrain height, and the TWP's for each grid point are direct outputs from the terrain analysis program. The terrain surface roughness value for each square kilometer is obtained independently from an analysis of the type vegetation and terrain surface for the region. MacArthur and Haines (1981) discuss techniques for calculating surface roughness. Other meteorological input necessary to run the surface wind model is also shown in Table 1. This input includes the free atmospheric wind, temperatures, heights and surface temperatures on a four point grid bounding the region of interest. In addition, latitude, time of day, day of year, percent cloud cover, sea breeze data (if appropriate), atmosphere transmissivity and program control variables are also required.

The following sections describe the three main components of the surface wind model: the calculation of the general surface wind, the local terrain influences on the wind, and the interpolation of the wind field to a uniform output grid.

TABLE 1

INPUT FOR SURFACE WIND MODEL

Input Supplied From Terrain/Wind Data Base

- Wind Computation Grid, $\{x_i, y_i, z_i\}$ $i = 1, \ldots, N$. This is the nonuniform grid computed by the Terrain Gridding Package
- Terrain Wind Parameters (TWP's) at each point i on the wind computation grid
- Surface Roughness Field. Aerodynamic surface roughness length for each square km of the analysis region
  $\{x_i^p, y_i^p, z_{o_i}^p\}$, $i = 1, \ldots, M \leq 2500$

Input Supplied By The User

- Switch to ignore initialization and allow direct input of general surface wind components U_b, V_b.
- UTM coordinates of the four corners of the region of interest $\{x_i, y_i\}$, $i = 1, \ldots, 4$. Alternatively, the SW corner point (x_c, y_c) and the length or width of the region.
- Free Atmosphere (850 mb) Wind, Temperature, and Heights, and surface temperatures on a four point grid bounding the region of interest

  $\{x_i^a, y_i^a, U_i^a, V_i^a, T_i^a, ZH_i^a, T_{sfc_i}^a, \}$ $i = 1, \ldots, 4$
- Latitude, ϕ_r, Time of day, t_d; Day of Year, Dy, for analysis region
- Percent Cloud Cover, C_c, and Transmissivity, P_B. Used to determine stability.
- Sea Breeze Data. Distance from analysis region (grid) center to shore of ocean (lake, etc.), d_b, and direction to shore, b_b. Direction is given in degrees counter-clockwise from East.
- Program Control Variables. Switches to activate the various modules containing the correction effects (sheltering, diverting, etc.)

- Output Grid. Uniform grid for presenting the output wind field. Given as the SW corner coordinates (x_o, y_o), the mesh length and width dimensions (Δx_o, Δy_o), and the overall grid dimensions (L_o, W_o). Also number of interpolation scans, initial radius of influence, percent reduction in influence radius for each succeeding scan, and the convergence criterion, which when satisfied terminates the interpolator.

2.2 THE GENERAL WIND AT THE SURFACE

The free atmosphere wind, at an altitude significantly above the influence of the terrain serves as the basic wind input parameter to the model. From the free atmosphere wind a surface wind field at 6 meters altitude is generated for each square kilometer. This general wind at the surface takes into account influences of the ground in flat terrain. Nonuniform terrain influences are accounted for in the next section.

Variation of wind speed and direction between ground and the free atmosphere is dependent upon surface characteristics (such as heating or cooling and roughness), the coriolis force, and the temperature structure of the intervening layer. The following scheme combines two methods to derive the 6 meter winds. The method of Gerrity, 1967, is used to deduce the 50 meter wind from the free atmospheric wind, and the Goodin and McRae (1980) method is used for the wind speed profile between the ground and 50 meters. The scheme is versatile since it incorporates both baroclinic shear as well as the effect of surface roughness.

Free atmosphere wind, temperature, height and surface temperature are specified on a four point grid surrounding the analysis region. These free atmosphere parameters are operationally available from National Weather Service or Air Force Global Weather Center weather charts. The following additional variables are needed to calculate the general wind at the surface:

- cloud cover and transmissivity for the region specified by the four points
- surface roughness for each sq. km in the analysis region.
- latitude, longitude, time of day, and day of the year.

First, the geostrophic wind components at the top of the constant stress layer and the Ekman turning of the wind between the free atmosphere and constant stress layer is obtained.

Gerrity's model divided the region between the earth's surface and the free atmosphere into two regions as shown in Figure 10. One is the constant stress layer near the earth's surface up to 50m where viscous forces dominate and the other is a transitional layer between the constant stress regime and the free atmosphere. In the free atmosphere pressure and rotational forces usually balance. Gerrity proposed that the geostrophic wind in the transitional layer could be modeled as

$$U_g = U_g^H + B(H-z) \tag{16}$$

$$V_g = V_g^H + C(H-z) \tag{17}$$

where U_g, V_g are the geostrophic components in the transition layer and U_g^H, V_g^H are the geostrophic components at the top of the transitional layer whose height is H. B and C are coefficients evaluated from the temperature field in the transitional layer and z is the altitude. More explicitly (16) and (17) can be written as

$$U_g = U_g^H + U_g^H \left(\frac{T_c - T_H}{T_H}\right) - \frac{gT_c}{f_o} \int_c^H \frac{\partial}{\partial y} \frac{1}{T} \, dz \tag{18}$$

$$V_g = V_g^H + V_g^H \left(\frac{T_c - T_H}{T_H}\right) + \frac{gT_c}{f_o} \int_c^H \frac{\partial}{\partial x} \frac{1}{T} \, dz \tag{19}$$

where T_c and T_H are the temperatures at the respective heights, c of 50 meters, and H, g is gravity, and f_o is the coriolis force for the latitude of interest. T_H is simply the free atmosphere temperature while T_c is 50 meter temperature derived from the surface temperature and an appropriate lapse rate.

A linear variation of temperature in the transitional layer is assumed. Thus, the vertical temperature profile is,

$$T(z) \equiv (T_H - T_c)(z - c) \,/\, (H - c) + T_c \quad . \tag{20}$$

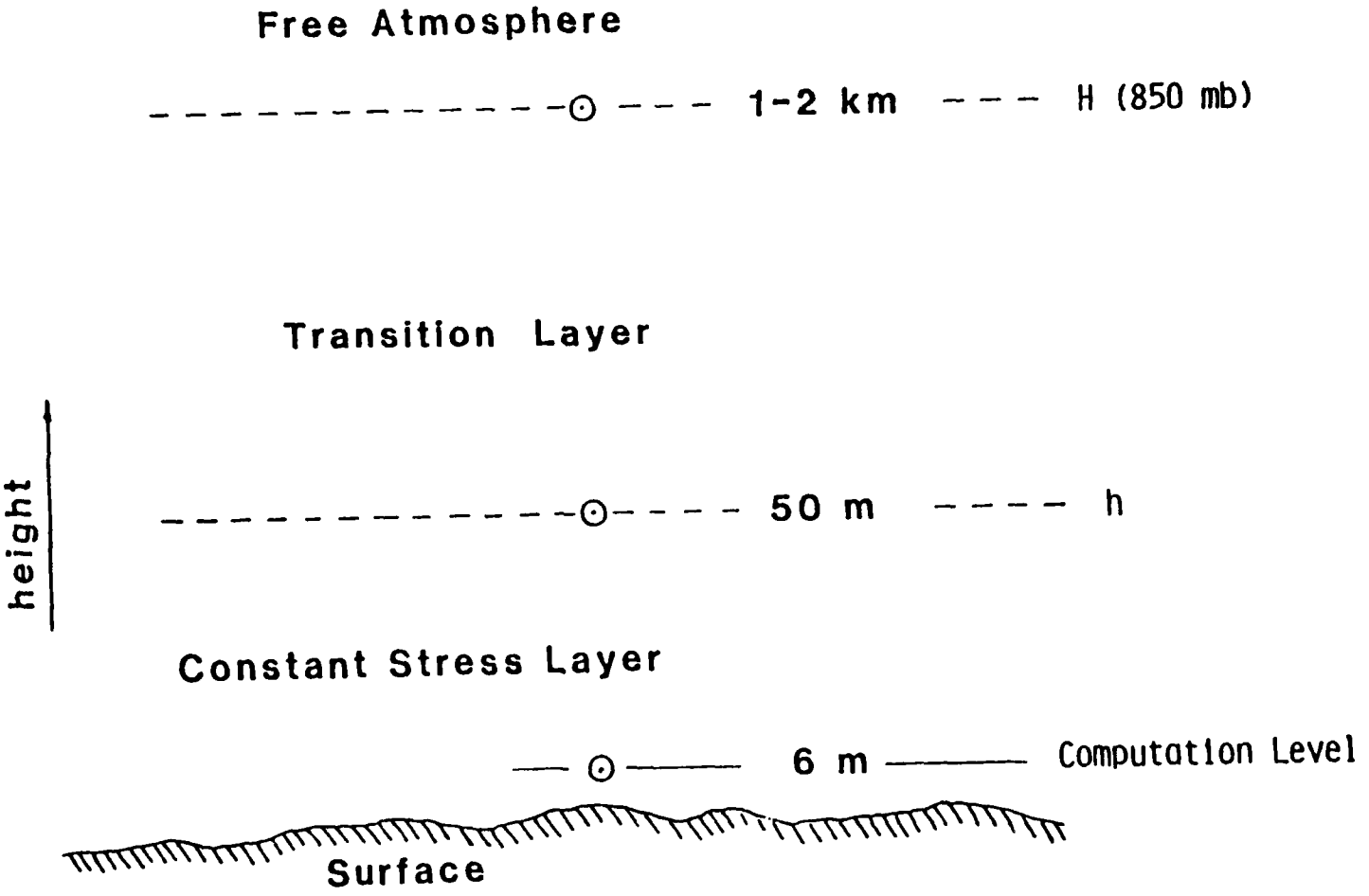

Figure 10. Two Part Division of the Planetary Boundary Layer.

Substitution of (20) into the integrals in (18) and (19) yields

$$\int_c^H \frac{\partial}{\partial y}\left(\frac{1}{T}\right)dz = \frac{\partial H}{\partial y}\ln\left[T_H/T_c\right] / \left(T_H - T_c\right)$$

$$+ \left(H - c\right)\left(T_c\frac{\partial T_H}{\partial y} - T_H\frac{\partial T_c}{\partial y}\right) / T_H T_c \left(T_H - T_c\right)$$

$$- \left(H - c\right)\ln\left[T_H/T_c\right] / \left(\frac{\partial T_H}{\partial y} - \frac{\partial T_c}{\partial y}\right)\left(\frac{\partial T_H}{\partial y} - \frac{\partial T_c}{\partial y}\right)^2 \qquad (21)$$

$$\int_c^H \frac{\partial}{\partial x}\left(\frac{1}{T}\right)dz = \frac{\partial H}{\partial x}\ln\left[T_H/T_c\right] / \left(T_H - T_c\right)$$

$$+ \left(H - c\right)\left(T_c\frac{\partial T_H}{\partial x} - T_H\frac{\partial T_c}{\partial x}\right) / T_H T_c \left(T_H - T_c\right)$$

$$- \left(H - c\right)\ln\left[T_H/T_c\right] / \left(\frac{\partial T_H}{\partial x} - \frac{\partial T_c}{\partial x}\right) / \left(\frac{\partial T_H}{\partial x} - \frac{\partial T_c}{\partial x}\right)^2 \qquad (22)$$

Resubstituting (21) and (22) into (18) and (19) and evaluating at z = c gives the geostrophic wind components at the top of the constant stress layer.

The geostrophic wind at the top of the constant stress layer can be corrected for the sea breeze influence. The magnitude of this effect depends on distance, d_b, and direction b_b to the ocean. Other details concerning the sea breeze remain as in the original Ryan model (1974).

The angular deviation, ψ, of the actual wind from the geostrophic, as the top of the constant stress layer is based on an empirical correlation with the surface Rossby number, R_o, Gerrity (1967),

$$\psi = a\left(\log R_o\right)^2 + b\left(\log R_o\right) + c \qquad (23)$$

where

$a = 0.625$,

$b = -12.75$,

$c = 80.625$,

$R_o = G/f_o z_o$, and

G = magnitude of geostrophic wind at 50m = $(U_g^2 + V_g^2)^{1/2}$.

f_o = coriolis force

z_o = surface roughness height

Table 2 below shows the variation of ψ with G and z_o for $f_o = 10^{-4}$/sec. Equation (23) is used to determine the wind direction at the surface from the direction of the free atmosphere wind.

Equation (23) is used to correct the wind direction at the surface (since no additional turning is considered to occur in the constant stress layer) for the influence of friction. It is currently formulated only for a neutral boundary layer. Angular deviation would be larger or smaller for respectively convective or stable boundary layers.

TABLE 2

Angular Deviation of the Constant Stress Layer Wind from Geostrophic

$\psi°$	R_o	G(m/sec)	z_o(m)	Description
39.6°	10^4	1	1	rough, light winds
34.5°	5×10^4	5	1	rough, moderate winds
32.5°	10^5	10	1	rough, windy
26.6°	10^6	1	10^{-2}	smooth, light winds
23.3°	5×10^6	5	10^{-2}	smooth, moderate winds
22°	10^7	10	10^{-2}	smooth, windy

The wind profile magnitude within the constant stress layer is based on stability and roughness. A quantitative measure of the stability influence (Liu et al., 1976) is based on the stress layer wind and insolation. Briefly σ is calculated as

$$\sigma = -1/2(3 - Cw + |Ce|) \text{ Sign } (Ce) \qquad (24)$$

where

$$Cw = \begin{cases} G/2, & 0 \leq G \leq 8\text{m/sec} \\ 4, & G \geq 8\text{m/sec} \end{cases} \qquad (25)$$

$$\text{Sign (Ce)} = \begin{cases} 1, & Ce > 0 \\ 0, & Ce = 0 \\ -1, & Ce < 0 \end{cases} \qquad (26)$$

$$Ce = \begin{cases} 3 & \text{strong} \\ 2 & \text{moderate} \quad \text{day time insolation} \\ 1 & \text{slight} \\ 0 & \text{heavy overcast } \} \text{ day or night} \\ -1 & \geq 4/8 \text{ cloud cover} \\ & \qquad\qquad \text{night time} \\ -2 & \leq 3/8 \text{ cloud cover} \end{cases} \qquad (27)$$

The algorithm for daytime Ce values is based on solar angle and cloud cover. The representation for σ is related to the Monin-Obuhkov length, L, and surface roughness z_o, by Liu et. al., as

$$L = \frac{z_o}{a_1\sigma + a_2\sigma^3}\left(b_1 - b_2|\sigma| + b_3\sigma^2\right) \qquad (28)$$

where

$a_1 = 0.004349$ $\qquad$ $b_1 = 0.5034$

$a_2 = 0.004724$ $\qquad$ $b_2 = 0.2310$

$\qquad\qquad\qquad\quad$ $b_3 = 0.0325$

If $\sigma = 0$, then $L = 10^6$m.

Following Goodin and McRae (1980), the surface friction velocity, u^*, is derived from the geostrophic wind, G, at the reference height z_r (50 meters) as

$$u^* = \frac{kG}{g_w} \tag{29}$$

where k is Von Karman's constant (0.35) and

$$g_w = \begin{cases} \ln \frac{z_r}{z_o} + 4.7 \left(\frac{z_r - z_o}{L}\right) & \text{stable or neutral } \frac{z}{L} \geq 0 \\ \ln \left[\frac{1 - \phi\left(\frac{z_r}{L}\right)}{1 + \phi\left(\frac{z_r}{L}\right)}\right] - \ln \left[\frac{1 - \phi\left(\frac{z_o}{L}\right)}{1 + \phi\left(\frac{z_o}{L}\right)}\right] & \text{unstable } \frac{z}{L} \leq 0 \\ + 2 \tan^{-1}\left[\frac{1}{\phi\left(\frac{z_r}{L}\right)}\right] - 2 \tan^{-1}\left[\frac{1}{\phi\left(\frac{z_o}{L}\right)}\right] & \end{cases} \tag{30}$$

where $\phi(z/L)$ a function related to wind shear is

$$\phi \frac{z}{L} \equiv \left[1 - 15\left(\frac{z}{L}\right)\right]^{-1/4} .$$

The integral form of the velocity gradient, Goodin and McRae (1980) is

$$u(z) = u(z_r) + \frac{u^*}{K} \int_{z_r}^{z} \phi \left(\frac{z}{L}\right) \frac{dz}{z}$$

which integrated is

$$u(z) = \frac{u^*}{k}\left\{ \ln\left(\frac{z}{z_r}\right) + \ln\left(\frac{\phi\left(\frac{z_r}{L}\right)^2 + 1}{\phi\left(\frac{z}{L}\right)^2 + 1} \; \frac{\left[\phi\left(\frac{z_r}{L}\right) + 1\right]^2}{\left[\phi\left(\frac{z}{L}\right) + 1\right]^2} \right) + 2\tan^{-1}\left[\phi\left(\frac{z}{L}\right)\right] - \tan^{-1}\left[\phi\left(\frac{z_r}{L}\right)\right] \right\} + u_r \qquad \frac{z}{L} < 0 \quad (31)$$

$$= \frac{u^*}{k} \ln \frac{z}{z_r} + u_r \qquad \frac{z}{L} = 0$$

$$= \frac{u^*}{k} \ln \frac{z}{z_r} + \frac{4.7\,(z-z_r)}{L} + u_r \qquad \frac{z}{L} > 0$$

Using $z = 6$ meters, $z_r = 50$ meters, we derive our general surface wind speed from equation 31. Derivation of the general surface wind is summarized in Figure 11.

2.3 LOCAL INFLUENCES ON THE GENERAL WIND

Predicting the surface wind speed and direction in complex terrain is a particularly difficult problem. The resultant wind at a given location arises from the interaction of different scales of motion-synoptic, mesoscale, and local. The problem can become quickly intractable if the interactions between various scales of motion are considered. To render the problem tractable, the assumption is made that second order interaction between various scales of motion can be neglected.

Diverse mechanisms are at work influencing the wind components in complex terrain. Synoptic scale influences which have already been considered arise from the large scale pressure gradient, the coriolis force, and surface friction. A mesoscale influence, the sea breeze, arises from land and sea temperature differences. The sea breeze is influenced by coriolis force and

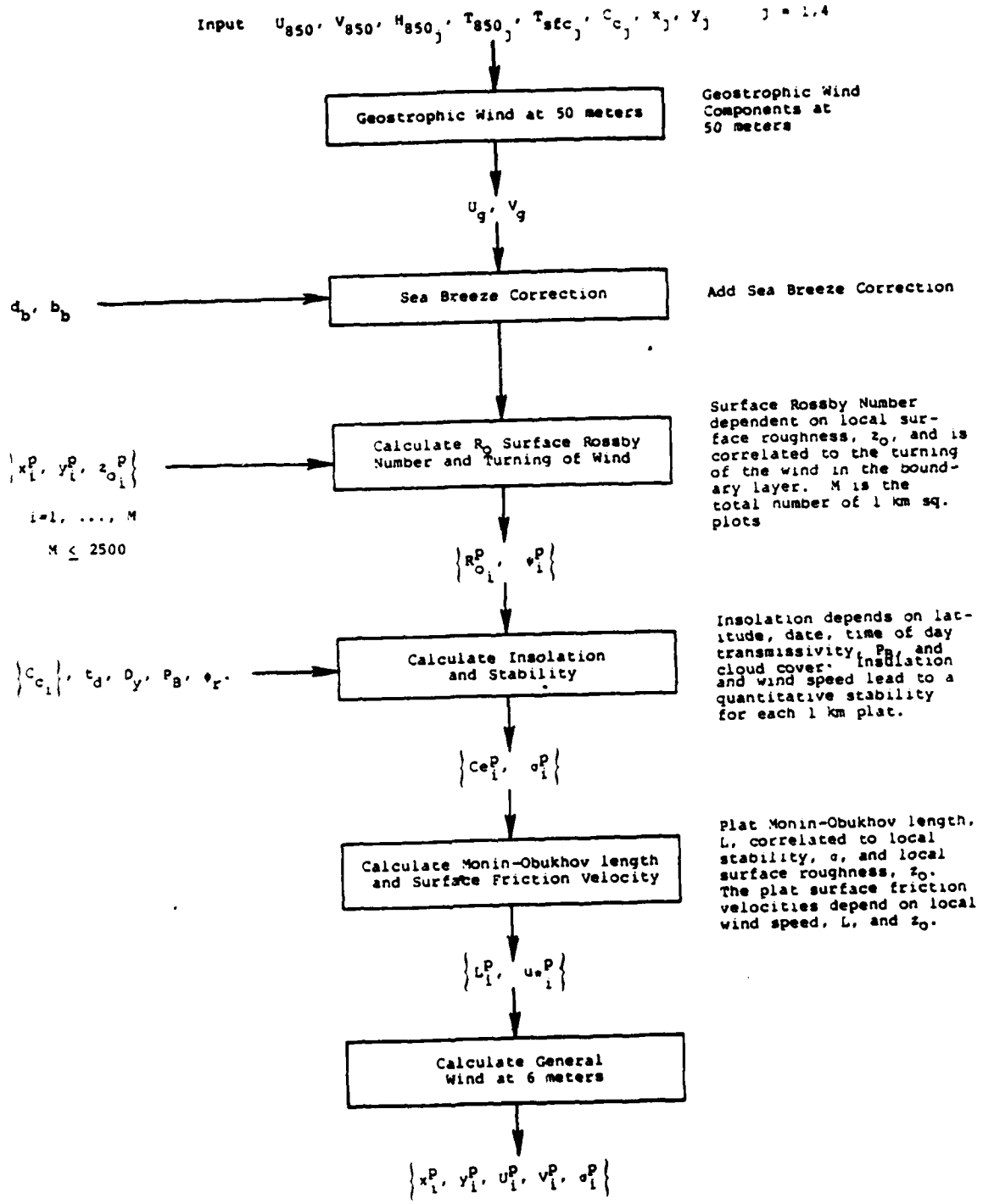

Figure 11. Steps in Calculating General Surface Wind from Free Atmosphere Wind.

friction as well. Nonuniform terrain features effect both synoptic and mesoscale flows by sheltering and diverting. The mean flow sheltering and diverting consist respectively of a decrease in wind speed in the lee of obstacles and a turning of the wind when it is obstructed. Synoptic scale and mesoscale flows are also affected in other ways by terrain. The flow over a ridge or hill speeds up according to the obstacle shape and slope. Flow separation over both ridges and hills is dependent on the terrain slope and atmospheric stability, but occurs at different values for hills (three-dimensional) and ridges (two-dimensional). The extent of separation beyond the obstacle is also different for hills and ridges. Nonuniform terrain also exerts local influences on the wind field. Slope and valley winds arise from the temperature differences due to uneven heating or cooling between the ground and air away from valley walls or mountain slopes.

Wind component variations over nonuniform terrain also occur in time. Diurnal and seasonal variations must be considered. Thus, the resultant wind in complex terrain consists of many terrain induced wind perturbations whose amplitudes vary in both time and space. A model for the local wind must incorporate both the space and time variations. The following sections describe each terrain induced perturbation and its influence at the 6 meter level.

2.3.1 Sheltering and Diverting

The general wind flow at a point in complex terrain is modified by sheltering and diverting. The decrease of wind speed on the lee side of a ridge at the 6 meter level due to sheltering is computed by a sheltering factor, F_u, (Ryan, 1974):

$$F_u = \tan^{-1}(.17Y_u)/100 \quad . \qquad (32)$$

where Y_u is the upwind slope to the horizon. This factor is based on Van Eimern's (1955) study of wind reduction by the

Harburg and Geest hills near Hamburg and Kaiser's (1959) study of wind speed reduction by shelterbelts.

The accompanying figure (12) lends additional support to Equation (32). Shown are the Van Eimern results for reduction of the wind speed in the Elbe Valley near Hamburg and the computed factor F_u from Equation (32). A curve was fit to this data that nearly parallels the F_u curve. Also shown are Counihan's (1969) results for the turbulent wake behind a rectangular block, which also favorably compares to F_u.

The surface wind speed is modified for sheltering by

$$W_{sd} = W_b - (W_b \cdot F_u) \tag{33}$$

where W_{sd} is the sheltered wind speed and W_b is the general surface wind speed from equation (31).

The wind direction is modified by a diverting angle, F_d, which depends on the surface wind direction at 6 meters, θ_b, aspect a, and slope Y_d of the terrain downwind. From Ryan (1974), the equation is:

$$F_d = -22.5 Y_d \sin[2(a - \theta_b)]. \tag{34}$$

Diversion is greatest, 22.5°, for a slope of 100% and an angle between aspect and wind direction of 45°. The diversion angle goes to zero as the wind either blows along or normal to the slope. The diverting angle corrects the general wind direction, θ_b, by

$$\theta_{sd} = \theta_b + F_d \quad . \tag{35}$$

Following Ryan, the east-west, U_{sd}, and north-south, V_{sd}, components of the surface wind modified for sheltering are

$$U_{sd} = -W_{sd} \sin \theta_{sd} \tag{36}$$

$$V_{sd} = -W_{sd} \cos \theta_{sd} \quad . \tag{37}$$

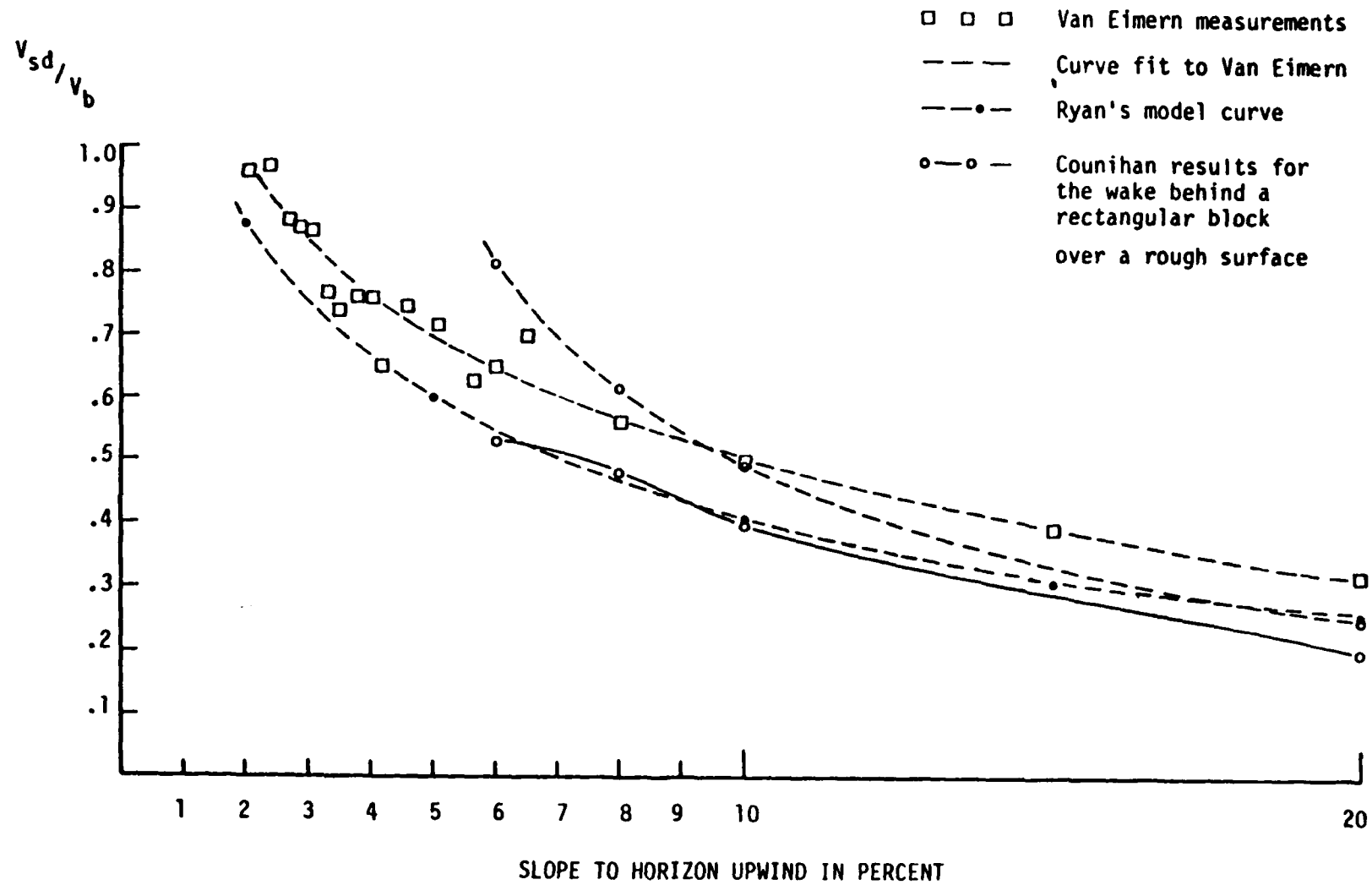

Figure 12. Comparison of Ryan Sheltering Equation with Measured Values.

We have associated a relative confidence factor with each local correction that is applied to the general surface wind. This confidence factor indicates the degree to which we believe the semi-empirical equations explain the actual phenomena. The relative confidence in the sheltering and diverting components of the wind is quite high, thus, we have weighted U_{sd} and V_{sd} by 1.0.

2.3.2 Slope Wind

In mountainous terrain either upslope or downslope winds are frequently observed. These winds arise from unequal heating or cooling of slope surfaces in comparison to air away from the slope at an equal altitude. The heating promotes positive buoyancy by day and negative buoyancy by night. Other influences such as adiabatic changes, slope of terrain, and nature of the slope surface affect the strength of this flow.

According to Petkovsek and Hocevar (1971), the nighttime slope wind strength parallel to a slope is

$$W_{ps} = \frac{C_1}{(\gamma_a - \gamma')\ (\sin(s))}\ \{1 - \exp[\frac{-g}{FT}(\gamma_a - \gamma')\sin^2 S\Delta t]\} \qquad (38)$$

where

W_{ps} = slope wind speed parallel to slope,

C_1 = diabatic cooling,

γ_a = adiabatic lapse rate,

γ' = atmospheric lapse rate outside cooled layer,

Y = slope to horizon

g = acceleration of gravity,

F = surface friction coefficient,

T = temperature outside cooled layer,

Δt = time since sunset or sunrise.

Petkovsek and Hocevar claim that winds calculated from (38) match data from observations well. Petkovsek and Hocevar's term "$(\gamma_a - \gamma')$" better models actual atmospheric lapse rate conditions than that of an earlier version (Fleagle, 1950) which considered the atmosphere outside the slope wind layer to be isothermal. Such a condition restricts the maximum values predicted by (38).

Ryan extended (38) to the daytime upslope condition by making the term C_1 apply to surface heating or cooling for respectively day and night. Ryan considered only the component of the slope wind in the horizontal plane. His equation is:

$$W_s = 2(I + C_n)\ (1 - C_p)\ /\ \tan S, \qquad (39)$$

where

I is solar insolation,

C_n is radiational cooling,

$C_p = \exp\left[-1.5\left(\frac{291.5}{T_{SURF}}\right)\ (\tan^2 S)\,\Delta t\right.$

S = local slope

and Δt is the time from the onset of either upslope or downslope flow. For upslope flow, Δt is the time from sunrise and for downslope flow it is the time from two hours before sunset. The factor $291.5/T_{SURF}$ accounts for the actual slope temperature which was a constant 291.5°K in Ryan's case studies.

The value of radiational cooling, C_n, according to Ryan is

$$C_n = .75 * P_B * (1 - \%\text{cloud cover}). \qquad (40)$$

where the transmissivity, P_B, was selected to be 0.7. This is appropriate to a moist boundary layer with some industrial particulates (Landsberg, 1969).

Insolation, I, is

$$I = I_o * P_B^{1/\sin C} * \sin\xi * (1 - \% \text{ cloud cover}) \qquad (41)$$

where I_o is the solar radiation at the top of the atmosphere, C is the angle of the sun from the horizontal and, ξ is the angle between the surface and the radiation path from the sun. More extensive discussion about both C and ξ is given in Ryan, 1974. The above equations from Ryan are used to calculate the upslope and downslope wind components.

The east-west component U_s and north-south component V_s of the slope wind are,

$$U_s = -W_s \sin a, \qquad (42)$$

$$V_s = -W_s \cos a \qquad (43)$$

Where a is the aspect.

Since the slope wind was originally formulated to model nighttime drainage winds and seems to do well in explaining drainage wind observations, the downslope wind confidence factor is 1.00. The confidence in the daytime upslope wind can not be as high since the vertical scale of the upslope wind is somewhat greater than its nighttime counterpart. As a result, the confidence in the upslope wind is set to 0.75.

2.3.3 Valley Wind

The valley or mountain wind is caused by temperature differences from above the valley to above the plain. This wind blows upvalley by day and downvalley by night. In the surface wind model the valley wind is based on an extensive series of observations conducted by Davidson and Rao (1957). They concluded that the valley wind strength appeared to be a function of valley width and depth and blew from the valley to the plain irrespective of valley slope. Their conclusions are further verified by the observations of Buettner and Thyer (1965) for winds in a mountain valley near Mt. Rainier.

Ryans's (1974) expression for the valley wind at 6 meters elevation is

$$W_v = (\bar{V}_v + 10.00 \sin (15t+244) + 1.69 \sin (30t+51.2)] \cdot P_B \cdot \bar{Y} \quad (44)$$

where

t is the time of day,

$\bar{V}_v = .89 + \sin (.986D + 79.88)$ is an amplitude that depends on day of year, D,

$\bar{Y}$ is average of left, Y_ℓ, and right, Y_r, slopes to the horizon.

P_B is the transmissivity

V_v is the magnitude of the valley wind in the valley direction, θ. The east-west and north-south components are given by

$$U_v = -W_v \sin \theta \quad (45)$$

$$V_v = -W_v \cos \theta \quad (46)$$

This empirical fit was designed to yield an upvalley wind speed for presumably optimum conditions. These occur in a well defined valley at the summer solstice. At mid-day the optimum wind speed corresponds to observed winds in a Southern California Mountain Valley. Equation (44) gave reasonable values for the Mt. Rainier valley winds as well. Because of the good agreement that the model valley wind had with Buettner and Thyer's observations, the valley wind confidence factor is 1.0.

2.3.4 Ridge Enhancement

Speed up or ridge enhancement of flow over hills and ridges is a commonly observed phenomenon that is especially crucial to a realistic surface layer wind model. Jackson and Hunt (1975) analytically determined the increase in wind speed

for an adiabatic turbulent boundary layer over a uniformly rough low two-dimensional hill ($h_s/l_s < .05$, where h_s and l_s are respectively the characteristic height and length of the hill.) Their solution predicts a "speed-up factor" $\Delta\Sigma$ at the top of the hill of

$$\Delta\Sigma = 2h_s/l_s \qquad (47)$$

Bradley (1978) reported observations of wind flow over a large hill in Australia. The size of the hill lay outside the range of validity for the Jackson and Hunt theory above, nevertheless, the observed speed-up agreed well with that predicted by (47). Bouwmeester (1978) further refined the estimates of ridge enhancement to include surface roughness and upwind and downwind slopes. Hunt (1980) reported several observations of speed up over ridges which substantiates (47). However for steeper hills or ridges, flow separation limits the speed up factor. Hunt further reported on the applicability of extending the two-dimensional result to three-dimensions.

Observations at Brentwood Knoll, a 130 m high three-dimensional round hill in southwest England, showed a speed-up factor of 2.2 to 2.3 as against a theoretical factor using equation (47) of 2.0. Other examples of three-dimensional observations which agree with two-dimensional results are given in Jackson and Hunt (1975).

In terms of the terrain wind parameters (TWP's) the speed up factor at the ridge crest is given as follows: in Figure 13 the hill height, h_s, is approximated as twice the vertical distance, DH, between the zero curvature point and the ridge crest. The hill length, l_s, as defined by Jackson and Hunt is estimated as the horizontal distance between the zero curvature point and ridge crest. In terms of the TWP's the speed up factor at the ridge crest is

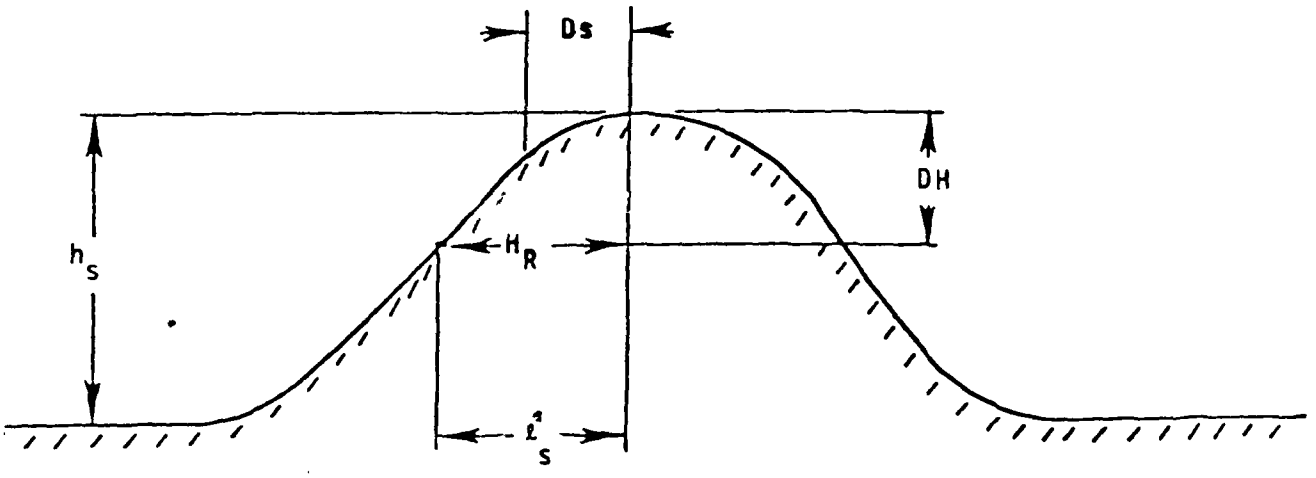

Figure 13. Comparison of Characteristic Hill Dimensions h_s and ℓ_s to the Hill Terrain Wind Parameters.

$$\Delta\Sigma = \frac{2h_s}{l_s} = \frac{4DH}{H_R} \qquad (48)$$

The calculated speed-up is strictly valid for the ridgecrest. Observations and modeling of wind flow over ridges and hills, however, show that faster flow is not solely limited to the very top of a ridge or hill. It extends over the entire top area. The exact functional form of the speed-up factor is not presently known. For purposes of modeling the variation of the speed-up factor from zero at some point on the lower hill or ridge to its full value at ridge or hill top, an exponential function $e^{-D_S/Hr}$ was constructed. The D_S represents the distance from the calculation point (x,y) to the ridge or hill top. The exponential factor models a decrease in the speed-up factor from its full value at ridge top to i/e at the distance $D_S - H_R$. If D_S exceeds H_R, the speed-up factor is zero.

$$\Delta\Sigma = \frac{4DH}{H_R} e^{-Ds/H_R}$$

where $s = \{(x - x_R)^2 + (y - y_R)^2\}^{1/2}$

Since a number of observations validate the theoretical speed up of ridge enhancement, the nominal confidence in it is set to 1.0. For points away from the ridge top, both the enhancement and confidence drop off. It is felt that an appropriate expression of the confidence is the exponential factor which spreads the enhancement over the ridge.

2.3.5 Flow Separation

Separated flow occurs in the lee of sufficiently steep terrain features. Its occurrence and extent is especially sensitive to the steepness of the feature and the atmospheric stability. In addition, separation is different for ridges and isolated hills. In the case of flow over a ridge, the streamlines form closed loops and the mean streamline from the separation point reattaches at the downwind end of the separation bubble as shown in Figure (14). For flow over a hill, the separation is much more complicated, some idea of the complexity can be seen in figure (15) which shows separated flow over a hill

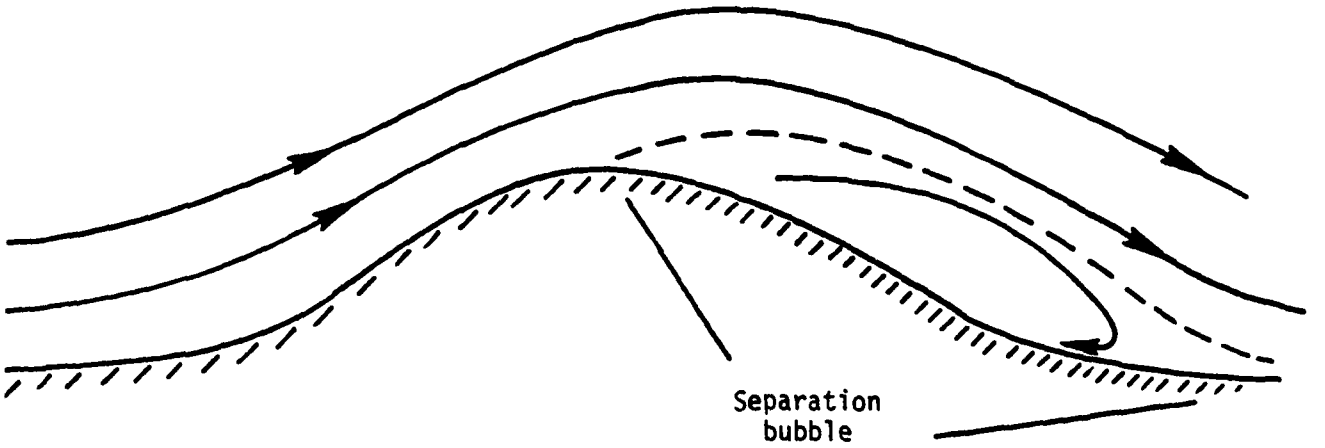

Figure 14. Two-dimensional Flow Separation Over a Ridge.

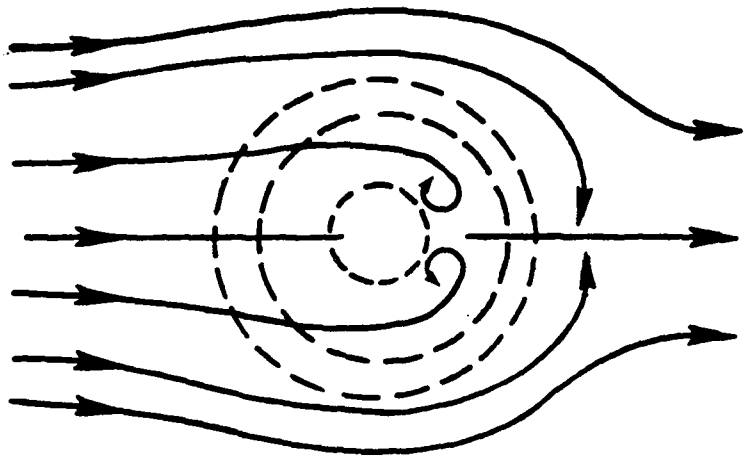

(a) Top view

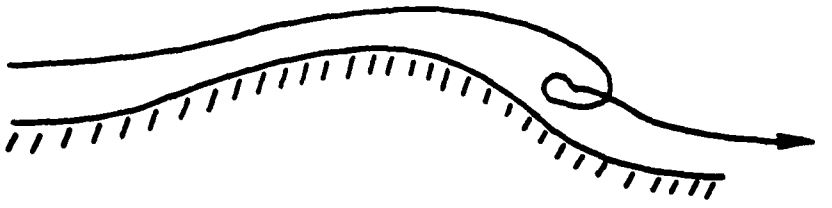

(b) Side view

Figure 15. Three-dimensional Flow Separation over an Isolated Hill.

viewed from above (a) and from the side (b).

Due to the differences between two and three-dimensional flow separation, the surface wind model calculates separation for ridges and hills differently. The algorithm that determines if a grid point is within a separated zone must first discriminate whether a hill or ridge lies upwind of the grid point. This discrimination is based on hill TWP's. Next, it must be determined whether or not separated flow is occurring, and finally, whether or not the grid point lies within the separation bubble.

The algorithm discriminating a three-dimensional hill from a two-dimensional ridge compares hill TWP's in three directions. For a ridge, the ratios of hill height to hill length, DH/H_R, both 45° to the left and 45° to the right of the grid point in the upwind direction must be at least 75% of the upwind value. Otherwise, with a positive DH/H_R, a hill is assumed.

In the case of a ridge, separation is based on whether the boundary layer is convective or neutral/stable. For a neutral/stable layer two criteria, for separation, and full separation, are used. The separation criterions:

$$\frac{DH}{H_R} > 0.04 + N_B^2 * 500. \qquad (49)$$

where N_B^2 is the Brunt-Vaisala frequency squared. N_B^2 is based on the stability and the surface temperature. The criterion for full separation, or maximum extent of the separation region is

$$\frac{DH}{H_R} > 0.06 + N_B^2 * 600. \qquad (50)$$

The downstream length of the separated flow at full development is 10 hill heights. With less than full development a proportion of the 10 hill height distance is used. This proportion is equal to the ratio of the DH/H_R exceedance of the separation criterion

to the difference between the criteria for full separation and separation. The separation criterion for a convective boundary layer is arbitrarily set to 0.05. For a convective boundary layer, the separated flow is arbitrarily considered to extend downstream for 5 hill heights.

For a three-dimensional hill, separation is assessed according to the results of Bouwmeester (1978). Separation occurs for hills with lee slopes greater than 0.28 in all atmospheric stabilities. The extent of separation is related to the hill Froude number,

$$F_h = W_b/N_B\ H_R \qquad (51)$$

where W_b is the general surface wind magnitude and H_R is the hill height TWP. According to Bouwmeester for F_h greater than 10, and a neutral/stable boundary layer the separated flow extends 10 hill heights downstream. Otherwise, the separation distance, SD, is related to the Froude number by

$$SD = (3 + F_h * 1.21) * D \qquad (52)$$

For a convective boundary layer, the surface wind model arbitrarily sets the separation distance at five hill heights.

When a point is found within a separated flow region based on the hill TWP's upwind, a diagnostic message is ouput and the confidence factor in the calculated wind reduced. This reduction is effected by adding the general wind magnitude to the denominator in the overall confidence factor calculation (see next section). In all cases, the relative confidence factor in separated flow is zero, but no change in the calculated wind is made.

2.3.6 Resultant Wind and Confidence Factor

For each grid point the relevant wind perturbation for sheltering and diverting, slope wind, valley wind, ridge

enhancement, and separation are calculated and decomposed into U and V components. At this time the perturbation due to separation is ignored. The magnitude and direction of the resultant wind after accounting for the other four components is calculated as

$$W = \left[\sum_{i=1}^{4} U_i^2 + \sum_{i=1}^{4} V_i^2 \right]^{1/2}, \text{ and} \tag{53}$$

$$\phi = \tan^{-1} \left(\frac{\sum_{i}^{4} U_i}{\sum_{i}^{4} V_i} \right), \tag{54}$$

where U_1, V_1 = surface wind components after accounting for sheltering and diverting

U_2, V_2 = perturbation components due to slope wind

U_3, V_3 = perturbation components due to valley wind

U_4, V_4 = perturbation components due to ridge enhancement

A resultant confidence factor is also derived; it includes an additional component assigned in case of flow separation. The expression for the confidence factor is

$$\text{Confidence} = \sum_{i=1}^{5} CF_i SP_i \; / \; \sum_{i=1}^{5} SP_i \tag{55}$$

where

CF_1 = confidence in sheltering diverting components

CF_2 = confidence in slope wind

CF_3 = confidence in valley wind

CF_4 = confidence in ridge enhancement

CF_5 = confidence in separation

and

SP_1 = Speed of sheltering - diverting wind
SP_2 = Speed of slope wind
SP_3 = Speed of valley wind
SP_4 = Ridge enhancement speed
SP_5 = General wind speed, assigned in case of separation.

2.4 INTERPOLATOR

The resultant surface winds lie on an optimized nonuniform grid as derived from the terrain processing routines. The use of the surface winds may be facilitated by conversion to a uniform grid whose spacing and location need not correspond with that of the nonuniform grid. The objective analysis of Cressman, (1959) was selected to produce a uniform grid because of its versatility and computational efficiency.

Input to the interpolation routines includes the location of the nonuniform grid points, the wind components, and the confidence factor at each grid point. The geographic location, extent, and spacing of the uniform grid are also required. Finally, the radius of influence, number of interpolation scans, percent of the influence radius to be used on each scan, and convergence criterion for an acceptable analysis are needed.

The objective analysis requires a first guess field which if good reduces the number of objective analysis scans necessary for convergence. In the case of surface winds, the first guess wind fields for each wind component and for the confidence factor is a constant: the mean of the nonuniform grid wind components and confidence factor fields. Specifically

$$U_o = \sum_{i=1}^{N} U_i/N \tag{56}$$

$$V_o = \sum_{i=1}^{N} V_i/N \tag{57}$$

$$CF_o = \sum_{i=1}^{N} CF_i/N \ , \tag{58}$$

where N is the number of non-uniform grid points.

The first guess field is then exposed to the "observation" (nonuniform grid) points. The determination of a uniform grid value of surface wind considers all the nonuniform point values within the radius of influence. The difference between a uniform grid value and "observation" value constitutes an interpolation error E for each component. For the U component, for example:

$$E_j = U_o - U_j$$

Each error is then weighted by the distance between the uniform grid point and "observation" point. The weighting function for each non-uniform observation point is

$$W_j = \frac{R_f^2 - d_j^2}{R_f^2 + d_j^2} \tag{59}$$

where d_j is the distance between the grid point and the observation point and R_f is the radius of influence. The radius of influence is generally chosen so that at least one nonuniform point is within R_f at any uniform point. The interpolation correction, C, applied to each wind component (or confidence factor), C, at a uniform point consists of the mean of the products of interpolation error times weighting factor or

$$C = \frac{\sum_{J} C_j}{J}$$

where

$$C_j = -W_j E_j$$

and J is the number of non-uniform grid points within the radius of influence.

The correction is applied to each component as

$$U' = U_o - C \tag{60}$$

$$V' = V_o - C$$

$$CF' = CF_o - C$$

Applying corrections (60) at each uniform grid point constitutes one interpolation scan. In subsequent scans, the influence radius is reduced by a specified percentage to enhance localized features. Between each scan a smoothing function is applied to each wind component and to the confidence factor. The smoothing function in terms of the U component is:

$$\bar{U} = 1/2\ U + 1/8\ \Sigma\ U_i \tag{61}$$

where $\Sigma\ U_i$ denotes the sum of the values at the four nearest grid points. Application of (61) serves to prevent discontinuities from arising in data sparse areas.

Normally a maximum of five scans is necessary to perform an analysis. After each scan, the maximum correction during that scan is compared to a convergence criterion. If the criterion is satisfied, the analysis is terminated and the results output. The steps in the analysis are summarized in figure 16.

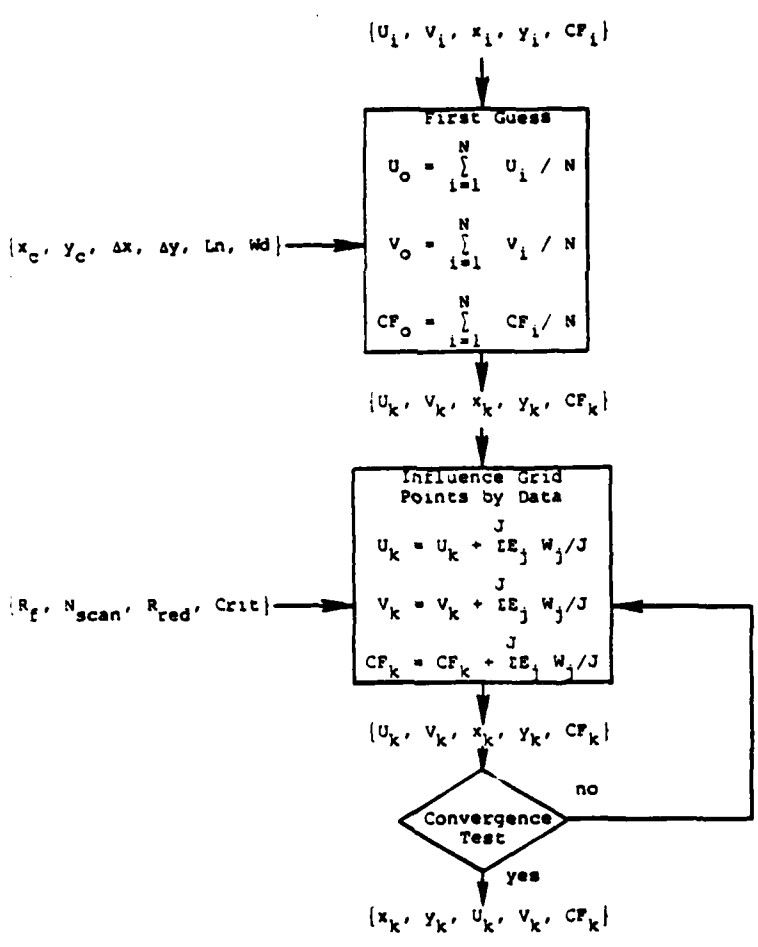

Notes

Local surface winds and confidence factor for non-uniform grid.

First guess components are means of input data. Uniform grid is derived by SW corner point, the mesh dimensions, and the length and width.

The subscript, k, refers to the uniform grid field.

Weighting is dependent on distance between grid points if within radius of influence. Influence radius must be "tuned" according to application.

Test for satisfactory convergence. Convergence occurs when the maximum correction in the field is below a tolerance criterion. If not, the grid values U_k, V_k are again subjected to an additional correction scan.

Figure 16. Interpolation of Local Surface Winds to Uniform Grid.

SECTION 3
RESULTS

This section presents four examples of surface winds calculated by the SWM for a region of complex terrain in Central Europe. The examples were chosen to isolate mechanical and thermal influences on the local wind under typical weather scenarios for the region. In these examples the general surface wind was specified and not derived from the free atmosphere winds. Examples for both winter and summer are included.

Figures 17 and 18 show respectively the nonuniform and uniform output grid of winds calculated for a high value of the general surface wind. For convenience a template showing the terrain in the example region is included with each set of figures. Conditions are for a winter night with clear sky and an easterly general wind of 10 m/sec. These conditions highlight ridge enhancement which is especially evident along the lower left edge of the figure as well as just to the upper right of the figure center. Sheltering is also evident in the lower figure center. A careful look at the lower right hand corner will reveal slight diversion of flow.

In contrast Figures 19 and 20 show respectively the nonuniform and uniform grid of winds for a light wind condition. The conditions are the same as for Figures 17 and 18 except the general wind was easterly at 1m/sec. With these conditions, weak but very evident slope winds appear. An especially good example is in the lower right corner where slope winds diverge from a hill top. The valley wind was too weak in this case to make an appearance. This is consistent since a well defined valley is not present in the region.

Figures 21 and 22 again show the nonuniform and uniform grid of winds for a high wind condition. In this case we have a summer day with clear skies and a northwesterly general wind at

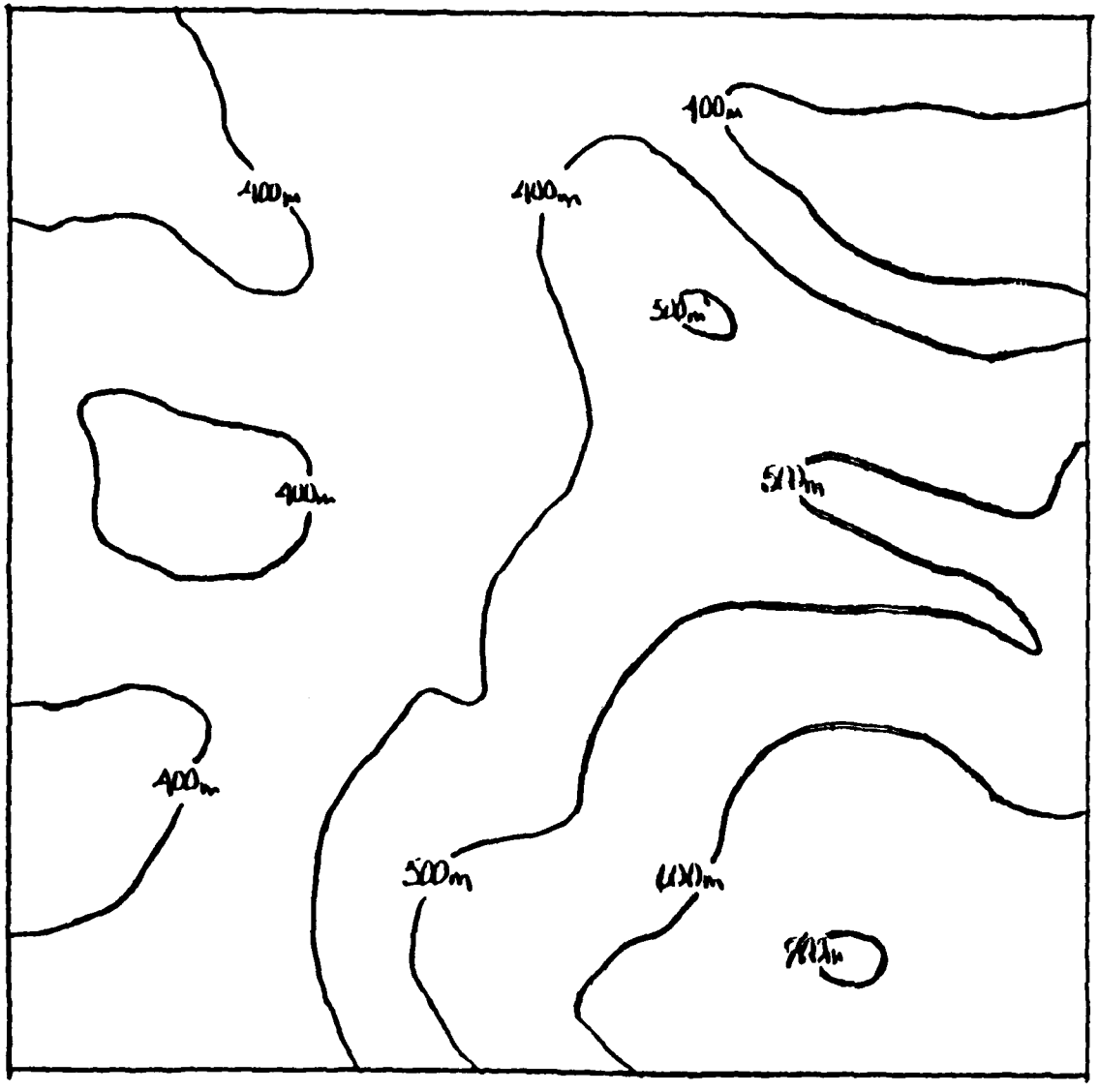

Terrain Overlay - RAW Height Field.

OPTION?

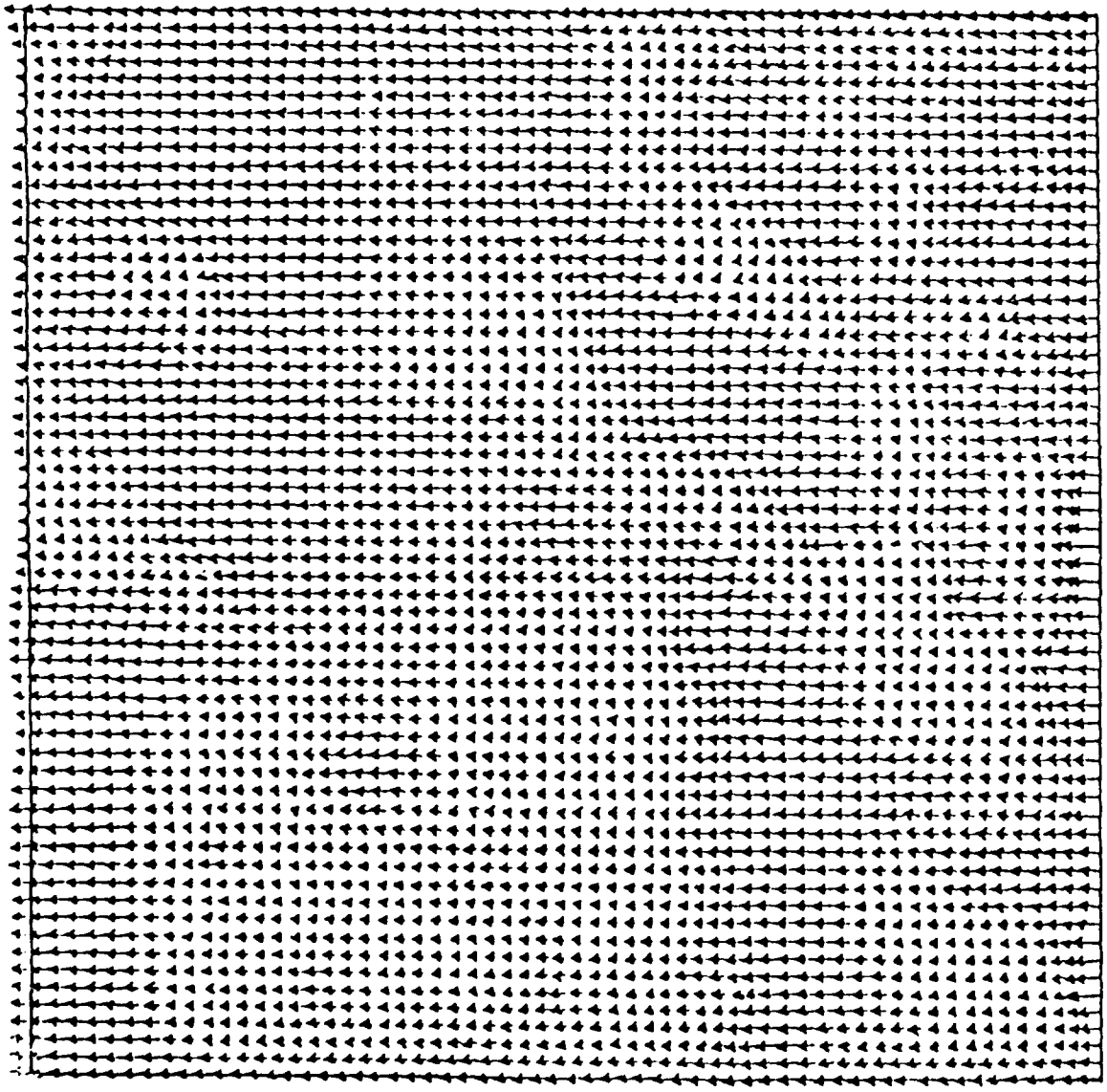

→
Arrow Length = 15 m/sec

Figure 17. Surface Wind Field's Uniform Grid, Winter Night, Clear Sky, 10 m/sec Easterly General Surface Wind.

OPTION7

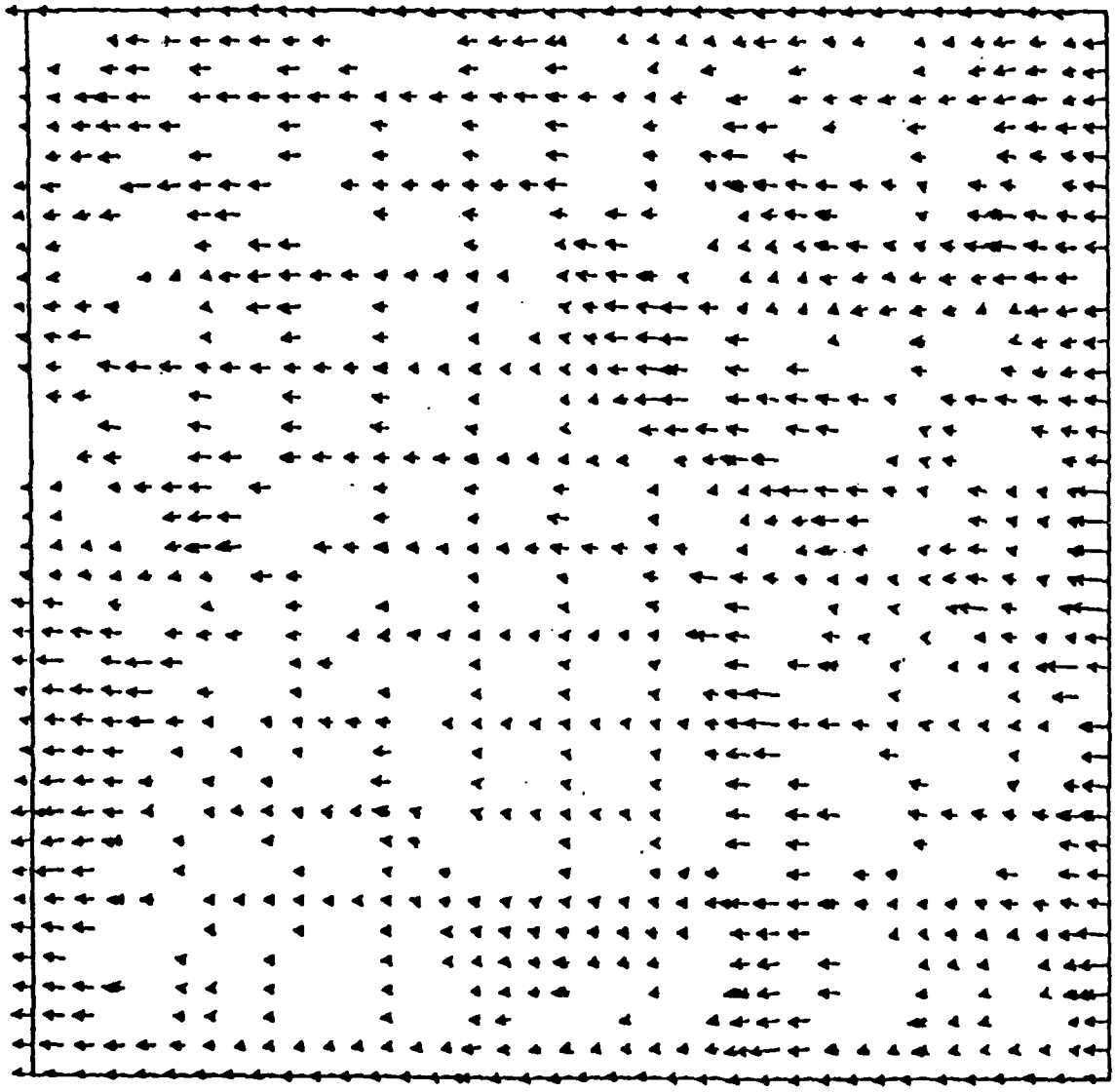

→

Arrow Length = 15 m/sec

Figure 18. Surface Wind Field, Non-uniform Grid, Winter Night, Clear Sky, 10 m/sec Easterly General Surface Wind.

OPTION7

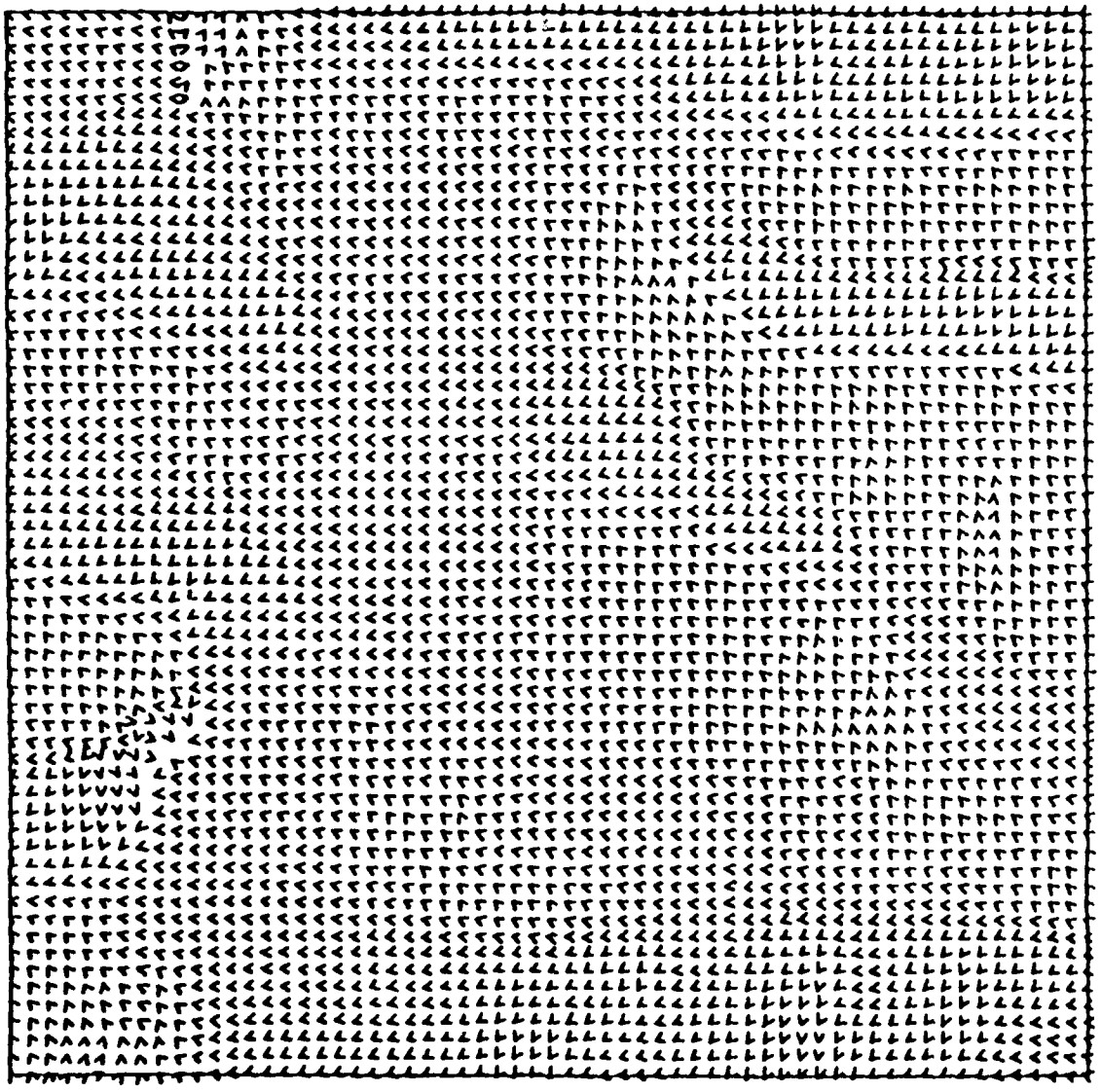

→

Arrow Length = 15 m/sec

Figure 19. Surface Wind Field, Uniform Grid, Winter Night, Clear Sky, 1 m/sec Easterly General Surface Wind.

OPTION?

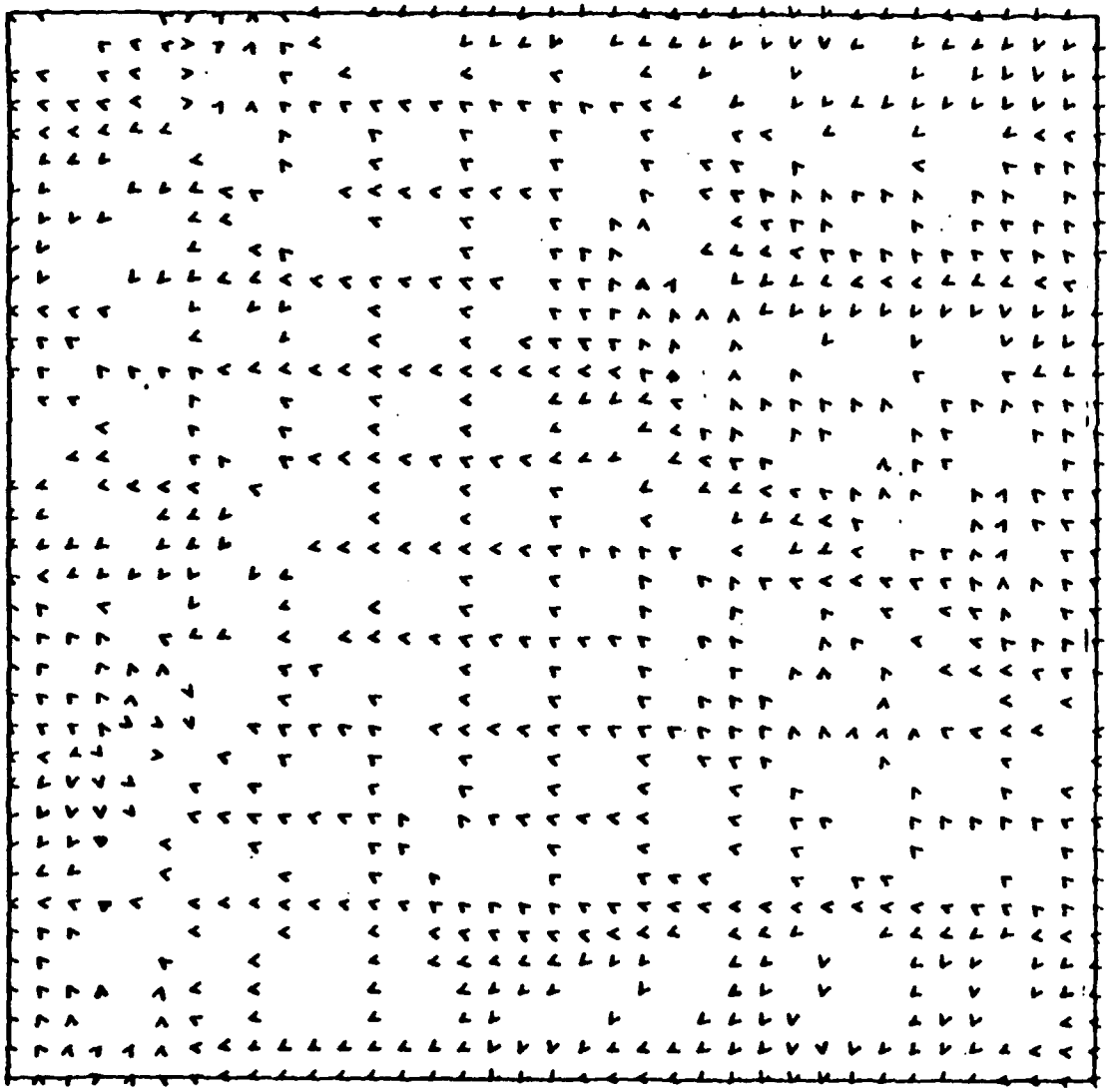

→

Arrow Length = 15 m/sec

Figure 20. Surface Wind Field, Non-uniform Grid, Winter Night, Clear Sky, 1 m/sec Easterly General Surface Wind.

OPTION?

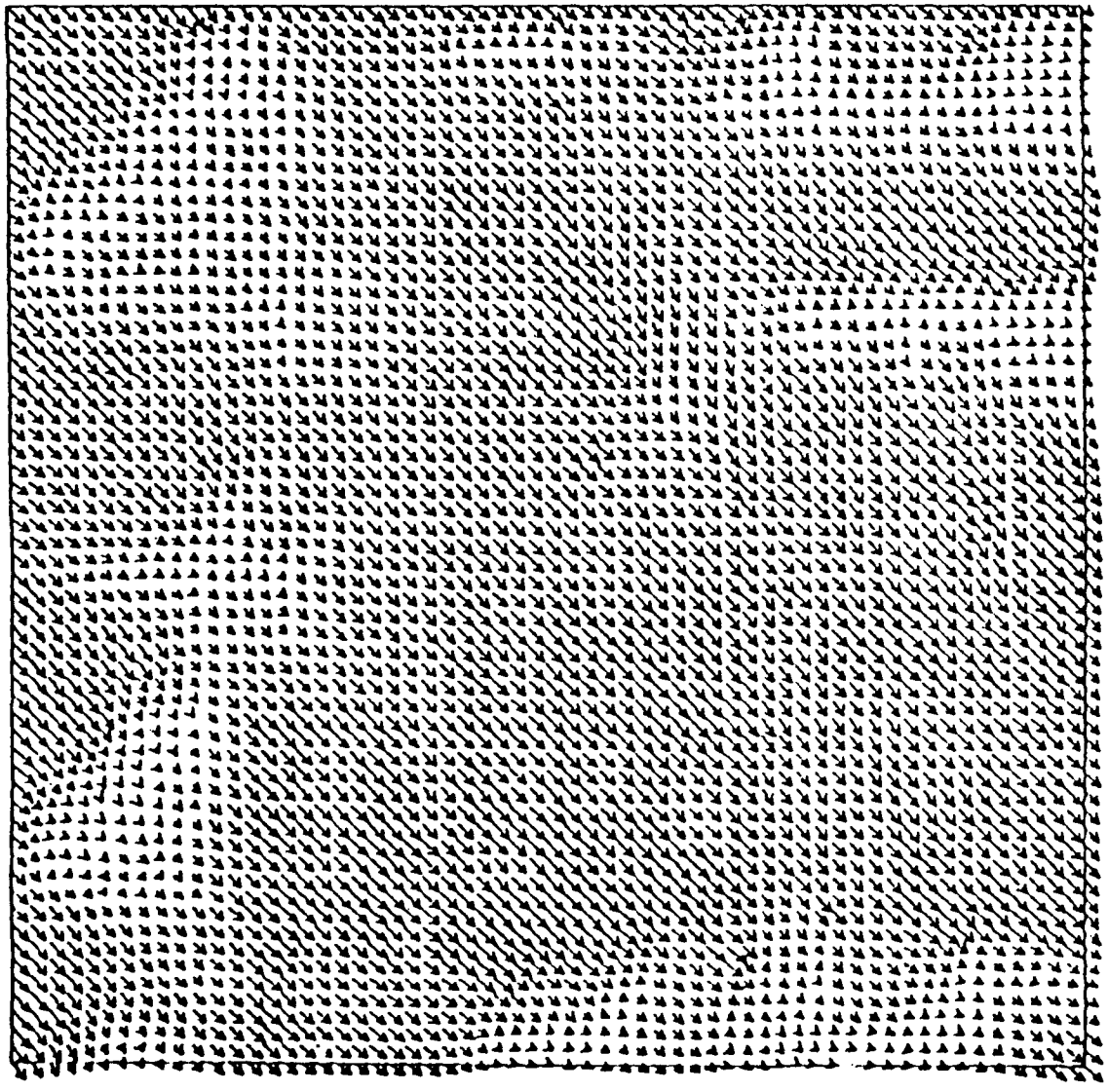

Arrow Length = 15 m/sec

Figure 21. Surface Wind Field, Uniform Grid, Summar Day, Clear Skies, 10 m/sec, North Westerly General Surface Wind.

OPTION?

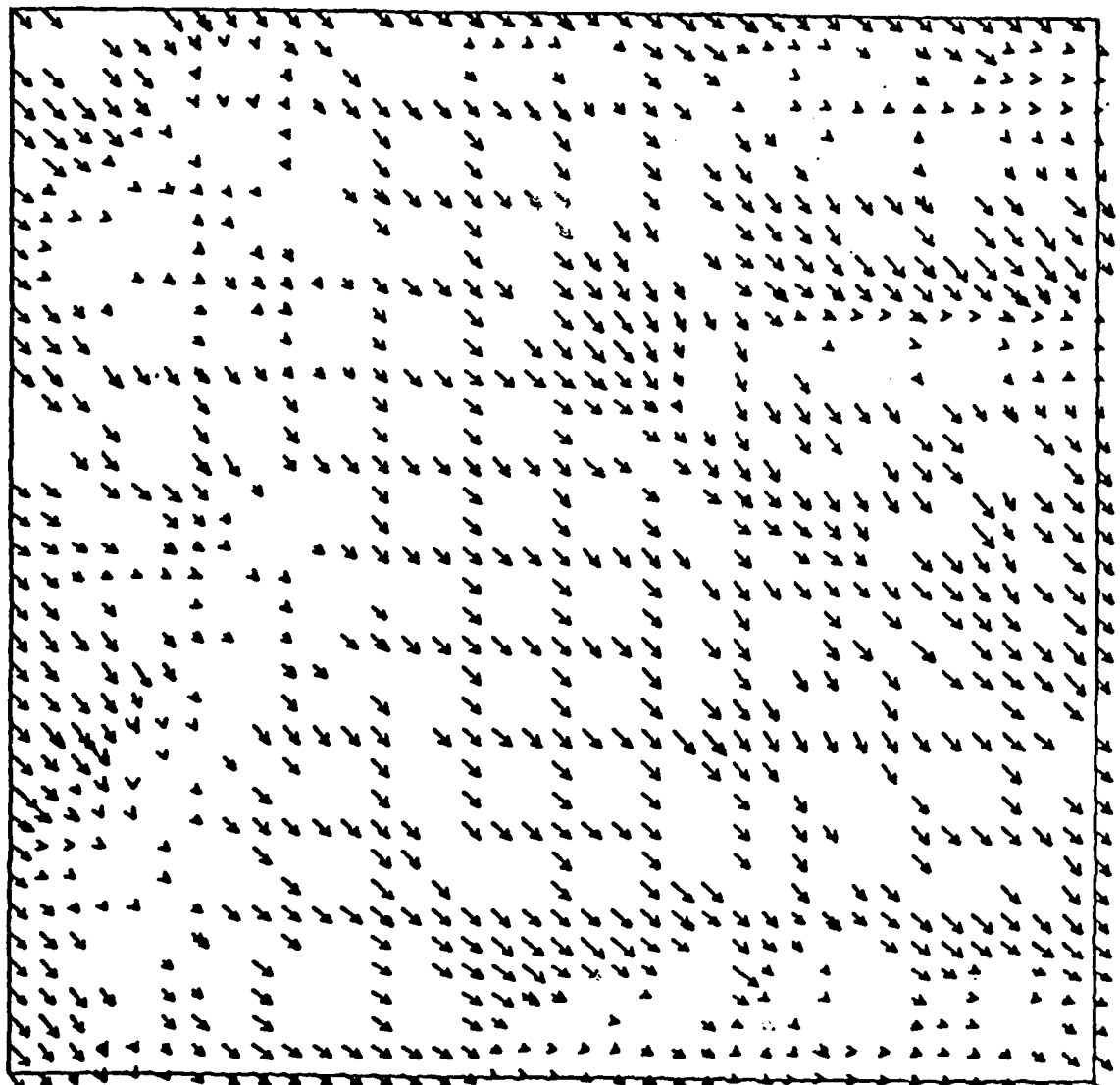

→

Arrow Length = 15 m/sec

Figure 22. Surface Wind Field, Non-uniform Grid, Summer Day, Clear Skies, 10 m/sec, North Westerly General Surface Wind.

10m/sec. Figure 22 is most interesting. It very clearly shows ridge enhancement in the upper left corner, just below middle along the left edge, lower left corner, just above the figure center, and below and to the right of center. Sheltering is also clearly evident in the figure's upper left corner, lower left bottom edge, upper right edge, and along the lower right bottom edge. These locations compare favorably with the topographic features of the region. Diversion is best seen in the lower and upper right corners.

Finally, Figures 23 and 24 are for light winds during a summer day. The sky is clear and the general wind is northwesterly at 1m/sec. The principal local wind influence is upslope winds perhaps best illustrated along the figures lower left edge. Again the valley wind appears too weak to show at this scale.

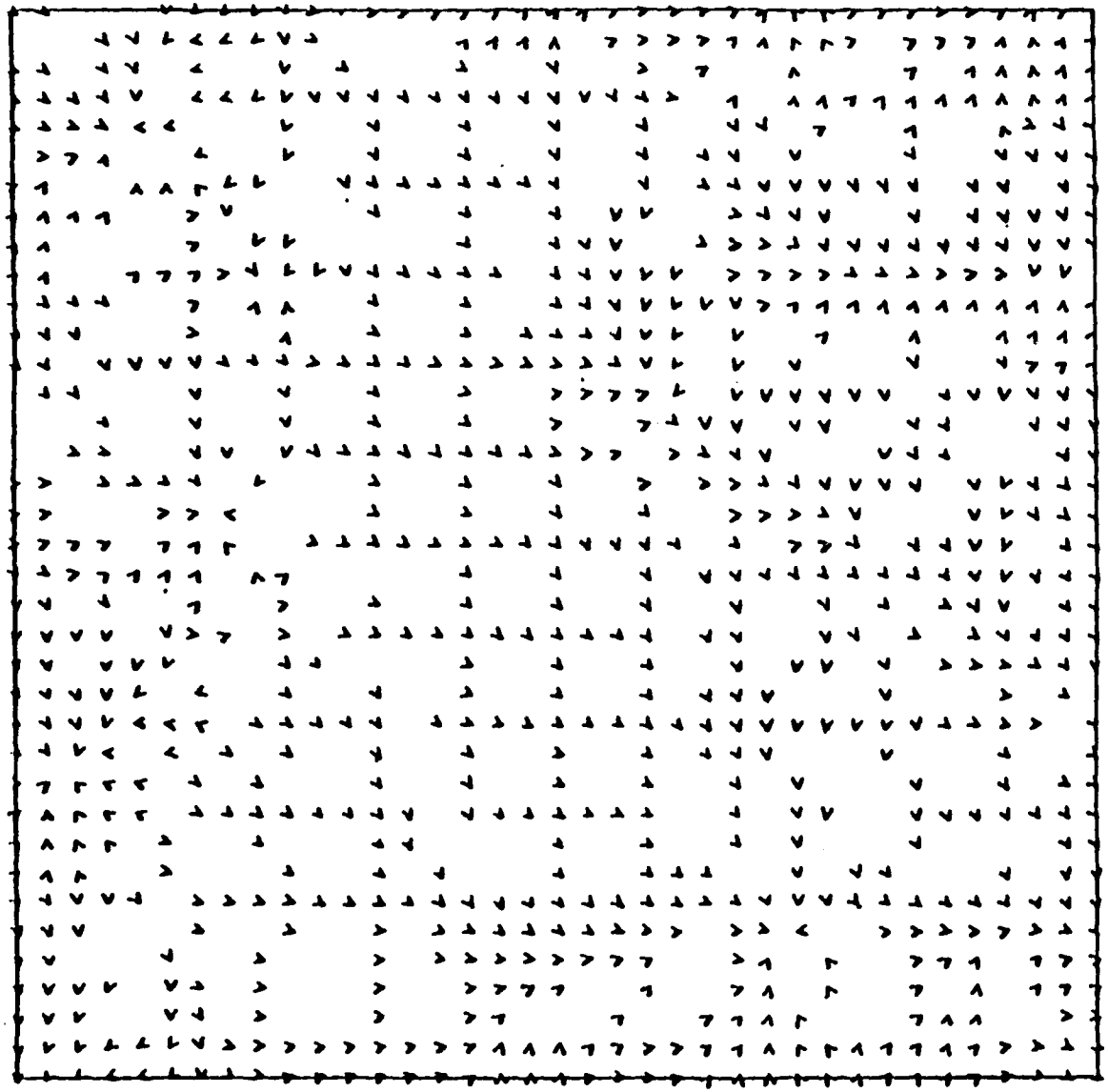

→

Arrow Length = 15 m/sec

Figure 23. Surface Wind Field, Non-uniform Grid, Summer Day, Clear Skies, 1 m/sec, North Easter. General Surface Wind.

OPTION7

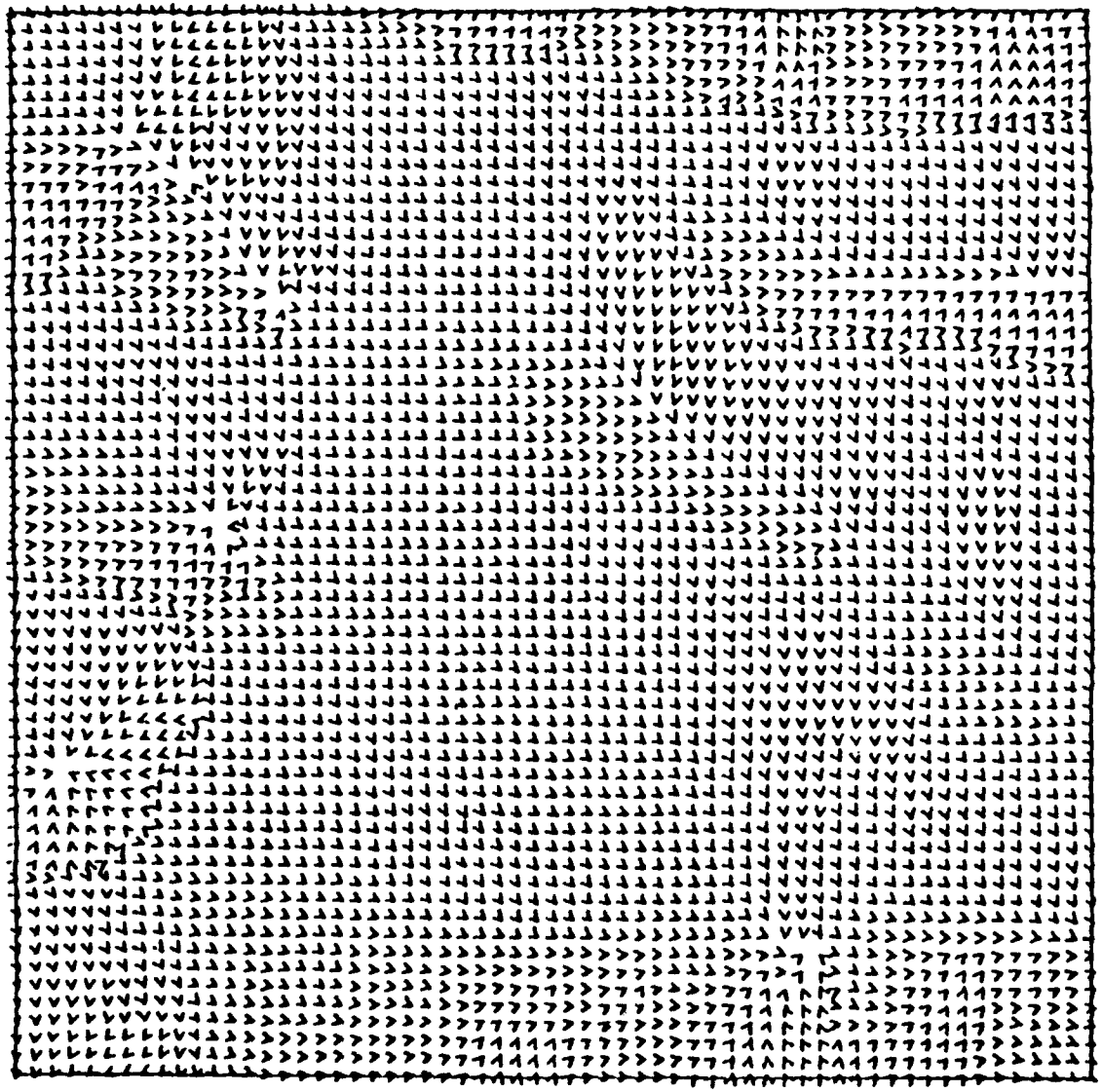

→

Arrow Length = 15 m/sec

Figure 24. Surface Wind Field, Uniform Grid, Summer Day, Clear Skies, 1 m/sec, North Westerly General Surface Wind.

SECTION 4
CONCLUSIONS

The preliminary exercises of the surface wind model have shown that it produces generally reasonable and expected results with good computational efficiency. It has been developed to a respectable degree of credibility as measured against the necessary tests of verification, validation, clarity of results, and workability. Some specific comments with respect to these elements of credibility follow.

4.1 VERIFICATION

The model possesses reasonable logical consistency. All components of the model owe their parentage to parameterization from tested empirical or theoretical studies. They have been systematically woven together to yield a methodology of considerable efficiency.

4.2 VALIDATION

The present model lacks detailed, rigorous testing against empirical data. However, the wind patterns, qualitatively, appear representative of those reasonably expected over complex terrain. The Terrain Wind Parameters can be expected to be quite satisfactory based on tests of the terrain fitting efficiency of the Tchebyshev representation. Average fit efficiencies are typically greater than 90% for 1 km windows, greater than 80% for 2 km windows and greater than 75% for 3 km window sizes. Standard deviations are typically a few percent.

4.3 CLARITY

The output can be viewed unambiguously and with a reasonable understanding of what processes are likely occurring. The vector plot approach appears to be a desirable format for presentation.

4.4 WORKABILITY

The surface wind model is cost effective and can be used to aid in decision making if desired. The existence of an analytical representation of the terrain surface allows for efficient calculation of terrain wind parameters. A 6 km by 6 km square area using a 1 km window requires less than one hour of CPU time on the UDRI DEC VAX11/780 to generate TWPs to calculate wind at about 150 m resolution. Furthermore, the TWP generation is a one-time-only exercise. Individual wind fields can then be calculated for numerous situations using less than five minutes of CPU time. This flexibility aids in its use as a decision making tool.

REFERENCES

Bouwmeester, R.J., 1978: Wind Characteristics Over Ridges. Ph.D. dissertation, Colorado State University, Ft. Collins, 233 p.

Boyd, J.P., 1978: The Choice of Spectral Functions on a Sphere for Boundary and Eigenvalue problems: A Comparison of Chevyshev, Fourier and Associated Legendre Expensions. Mon. Wea. Rev., 106, 1184-1191.

Bradley, E.F., 1980: An Experimental Study of the profiles of Wind Speed, Shearing Stress, and Turbulence at the Crest of a Large Hill. Quart. J. Roy. Meteor. Soc., 106, 101-124.

Buettner, K. J. K., and N. Thyer, 1965: Valley winds in the Mount Rainier Area. Archiv. fur Meteorologie, Geophysik und Bioklimatologie, 14 (2), 125-147.

Counihan, J., 1969: An Improved Method of Simulating an Atmospheric Boundary Layer in a Wind Tunnel. Atmos. Environ. 3, 197.

Cressman, G.D., 1959: An Operational Objective Analysis System. Mon. Wea. Rev., 87 (10) 367-394.

Davidson, B., and K. P. Rao, 1957: "Preliminary Report on Valley Wind Studies in Vermont." Final Report Contract AF 19 (604) 1971, Eng. Res. Div., New York Univ., 54 p.

Gerrity, J. P., 1967: A Physical, Numerical Model for the Prediction of Synoptic-Scale Low Cloudiness. Mon. Wea. Rev. 95, 261-282.

Goodin, W. R., and G. J. McRae, 1980: A Procedure for Wind Field Construction From Measured Data Which Utilizes Local Surface Roughness. Preprint Volume, Second Conference on Coastal Meteorology, 233-239.

Hunt, J. C. R., 1980: Wind over Hills. Workshop on the Planetary Boundary Layer, American Meteorological Society, Boston, 107-144.

Jackson, P.S., and J. C. R. Hunt, 1975: Turbulent Wind Flow over a Low Hill. Quart. J. Roy. Meteor. Soc., 101, 929-956.

Kaiser, H., 1959: Die Stromung an Windschutstreifen. Ber. Dstch. Wetterd., 7, 53.

Landsberg, H. E., editor, 1969. General Climatology, 2, Elsevier, New York, 266 p.

Liu, M. K., et al., 1976: "The Chemistry, Dispersion and Transport of Air Pollutants Emitted From Fossil Power Plants in California: Data Analysis and Emission Impact Model," Systems Applications, Inc., San Rafael, CA.

MacArthur, C. D., and P. A. Haines, 1981: The Roughness Lengths Associated with Regions of Heterogeneous Vegetation and Elevation, University of Dayton Research Institute.

Petkovsek, Z., and A. Hocevar, 1971: Night Drainage Winds. Arch. Meteor. Geophys. Bioklimatol., Ser. A., 20, 355-360.

Ryan, B. C., 1974: A Mathematical Model for Diagnosis and Prediction of Surface Winds in Mountainous Terrain. Ph.D. dissertation, University of California, Riverside, 135 p.

VanEimern, J., 1955: Uber eine Windbeeinflussung durch die Randhohen des Elbatals bei Hamburg. Meteor. Rundsch, 8, 97-99.


DATE
FILME
5-8